Journal of Medicinal Chemistry

pubs.acs.org/jmc Article

A Chemical Switch for Transforming a Purine Agonist for Toll-like Receptor 7 to a Clinically Relevant Antagonist

Ayan Mukherjee,[‖] Deblina Raychaudhuri,[‖] Bishnu Prasad Sinha,[‖] Biswajit Kundu, Mousumi Mitra, Barnali Paul, Purbita Bandopadhyay, Dipyaman Ganguly,* and Arindam Talukdar*

Cite This: *J. Med. Chem.* 2020, 63, 4776–4789 Read Online

ACCESS | Metrics & More | Article Recommendations | Supporting Information

ABSTRACT: Toll-like receptor 7 (TLR7) is an established therapeutic target in myriad autoimmune disorders, but no TLR7 antagonist is available for clinical use to date. Herein, we report a purine scaffold TLR7 antagonist, first-of-its-kind to our knowledge, which was developed by rationally dissecting the structural requirements for TLR7-targeted activity for a purine scaffold. Specifically, we identified a singular chemical switch at C-2 that could make a potent purine scaffold TLR7 agonist to lose agonism and acquire antagonist activity, which could further be potentiated by the introduction of an additional basic center at C-6. We ended up developing a clinically relevant TLR7 antagonist with favorable pharmacokinetics and 70.8% oral bioavailability in mice. Moreover, the TLR7 antagonists depicted excellent selectivity against TLR8. To further validate the *in vivo* applicability of this novel TLR7 antagonist, we demonstrated its excellent efficacy in preventing TLR7-induced pathology in a preclinical murine model of psoriasis.

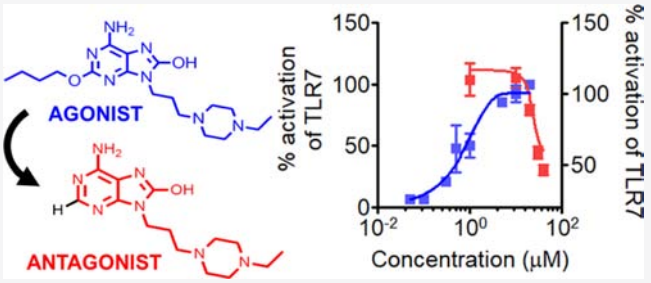

INTRODUCTION

Toll-like receptors (TLRs) are the critical first line of immune defense that are mostly expressed on antigen presenting cells, for example, dendritic cells and recognize molecular signature patterns associated with pathogens.[1−3] The members of the TLR family of receptors that can recognize nucleic acid molecules, both of self and nonself origins, *viz.* TLR7, TLR8, and TLR9, are located inside the acidic endosomal compartments of the immune cells.[2,4−6] Among them, TLR7, which recognizes single-stranded RNA, is expressed in humans selectively in plasmacytoid dendritic cells (pDCs) and B lymphocytes and when activated in pDCs drives type I interferon production from pDCs.[4] pDC-derived type I interferons (IFNs) are critical innate immune events in a number of autoimmune diseases, *viz.* systemic lupus erythematosus (SLE), psoriasis, Sjögren's syndrome, systemic sclerosis, and so forth.[7−11] Thus, the endosomal TLRs in pDCs, for example, TLR7, are important therapeutic targets for these clinical contexts.[12−14] Application of the TLR7 agonist imiquimod on the skin leads to cutaneous autoimmunity in mice, which mimics the human skin autoimmunity in psoriasis, and consequently is an established preclinical model for psoriasis.[15] However, a suitable TLR7 antagonist is yet to be available for clinical use.[16]

Both receptor agonists and antagonists are important therapeutic molecules in different clinical contexts and in many cases agonists and antagonists share overlapping binding region in their target molecules. Thus, agonistic chemical scaffolds are often used as a template for designing antagonists with shared region-specificities for the receptors,[17−19] for example, development of β-adrenergic receptor antagonists from the endogenous agonist adrenalin,[20] histamine receptor 2 antagonists from histamine,[21] and opioid receptor antagonists from opioids.[22] TLR7-mediated immune activation has implication in autoimmune diseases like SLE, psoriasis. In SLE autoreactivity against RNA and RNA binding proteins are very prevalent and these immune complexes activate TLR7 in both pDCs and B cells, thereby perpetuating the inflammatory cascade.[10] In psoriasis self-RNA molecules released by dying keratinocytes form complexes with cationic antimicrobial peptides. These complexes have been shown to activate both plasmacytoid and conventional dendritic cells thus fuelling the cutaneous inflammation.[8,10] Hence, blocking TLR7 activation with suitable antagonist is sought for, which may intercept one of the key pathogenic nodes in these diseases. Purine scaffold is extensively studied for its potent TLR7 agonist activity.[23−26] Interestingly, guanosine, an endogenous purine class molecule, is also an agonist for TLR7.[27] The mechanism of TLR7 activation by guanosine has been shown through crystallo-

Received: January 3, 2020
Published: April 17, 2020

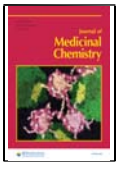

https://dx.doi.org/10.1021/acs.jmedchem.0c00011
J. Med. Chem. 2020, 63, 4776–4789

Scheme 1[a]

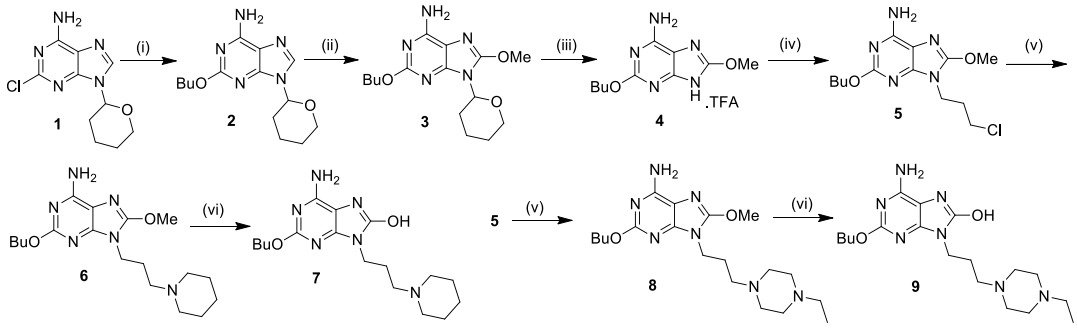

[a]Reagents and conditions: (i) sodium *t*-butoxide (4.0 equiv), *n*-BuOH, 100 °C, 12 h, 77%; (ii) a. *N*-bromosuccinimide (1.05 equiv), $CHCl_3$, 3 h, rt, b. sodium methoxide (2.7 equiv), CH_3OH, reflux, 4 h, 80%; (iii) 10% TFA in methanol, rt, 72 h, 73%; (iv) 1-bromo-3-chloropropane (2.0 equiv), potassium carbonate (2.6 equiv), rt, 16 h, 67%; (v) piperidine for compound **11** or ethylpiperazine for compound **12** (3.0 equiv), potassium carbonate (1.5 equiv), rt, 6 h, 67−73%; (vi) 4 M HCl in 1,4-dioxane, 3 h, 87−91%.

graphic study which is of great value in design and development of TLR7 ligands.[28] Previous efforts directed toward the purine scaffold have led to potent agonists' thorough understanding about the region-specificities of critical substituents. From crystallographic evidence and structural development of TLR7 agonist, it is understandable that the $-NH_2$ group at C-6 position is crucial for scaffold recognition by TLR7.[28] Thus, logically, we did not change the $-NH_2$ group at C-6 position in our initial SAR development. Development of 2-substituted-8-hydroxyadenine as IFNα inducer via TLR7 pathway revealed the profound effect of four carbon long alkoxy chain at C-2 position on the agonistic activity.[25,29] Among various substituents, O-alkyl groups at C-2 position have been found to have superior ability to modulate the agonistic activity in combination with *N*-benzyl or *N*-alkylamine at N-9 position.[30−32] Previous study on pteridinone core-based TLR7 agonist showed that C-2 position butoxy linker bind to the conserved hydrophobic pocket of TLR7.[33] The N-9 substitutions modulate both activity and pharmacokinetic profile of purine,[23,24] perhaps because the weak base gets protonated and trapped in the acidic endosomal compartment,[34,35] harboring TLR7. Throughout the literature, the C-2 position was substituted, and subsequently modification was done in N-9 position but not the other way round. Keeping this in mind, we intended to evaluate the fate of the agonist where the C-2 substituent is absent keeping the known relevant N-9 substituents and $-NH_2$ group at C-6 position. Although extensive focus has been devoted toward the development of TLR7 agonist, there is no reported TLR7 antagonist of purine scaffold, to our knowledge. Imiquimod belongs to imidazoquinoline class of molecules, which also includes other well-known TLR7 agonists like gardiquimod and resiquimod.[36] TLR7 agonist gardiquimod was successfully transformed into TLR7 antagonist by converting to its 3*H* regioisomer.[18]

We have initiated our study from a representative purine agonist **7** containing essential TLR7 agonistic features at C-2, C-6, C-8, and N-9. We have explored the minimal structural features that impart antagonism in compound **7**, for mapping the synthetic path to a novel purine scaffold antagonist. We have depicted that a small structural modification in the ligand can lead to major changes in their functional activity. For assessing the TLR7-targeted activity (both agonism and antagonism) of the molecules, we used engineered HEK293 cells that expressed exogenous human TLR7 and reported TLR7-induced NF-κB activation in a secreted alkaline phosphatase (SEAP)-driven colorimetric assay. We have used a nonselective TLR7 antagonist hydroxychloroquine as a positive control. Through SAR development, we identified clinically relevant TLR7 antagonist **23** that has favorable pharmacokinetic properties with 70.8% oral bioavailability in mice. The nature of antagonism was determined by subjecting these antagonists to agonism assay. The TLR7 antagonists reported herewith showed excellent selectivity against TLR8. *In vivo* efficacy of **23** was demonstrated by its ability to prevent TLR7-induced pathology in a preclinical murine model of psoriasis.

CHEMISTRY

Chemical Synthesis of TLR7 Agonist 7 and 9. C-6 position of compound **1**[30] was substituted with *n*-butoxy linkage via sodium *t*-butoxide treatment to obtain compound **2**. The methoxy group at C-8 was introduced by bromination of **2** using *N*-bromosuccinimide followed by refluxing with a 5 M solution of sodium methoxide in methanol to provide compound **3** (Scheme 1). Deprotection of pyran ring from compound **3** using 10% trifluoroacetic acid (TFA) followed by 3-chloropropyl substitution in compound **4** using 1-bromo-3-chloropropane yielded compound **5**. The chlorine group in compound **5** was then substituted with either piperidine or ethylpiperazine to give compounds **6** and **8**. Finally, C-8 position methoxy group was deprotected using 4 M HCl in 1,4-dioxane to get compounds **7** and **9**.

Chemical Synthesis of Weak TLR7 Antagonist 14. In the present Scheme 2, we successfully standardized a protocol for the synthesis of compound **14** by avoiding protection−deprotection chemistry at N-9 position in purine scaffold. Bromo group of 8-bromo adenine **10**[37] was substituted with methoxy group by refluxing with a 5 M solution of sodium methoxide in methanol to obtain compound **11**, which on treatment with 1-bromo-3-chloropropane provided compound **12**. Chlorine group was substituted by ethylpiperazine to yield compound **13** and that followed by deprotection of methoxy group gave compound **14**.

Chemical Synthesis of Potent TLR7 Antagonist. Substitution of 3-carbon linker with ethylpiperazine group at N-9 position of 6-chloropurine (**15**) resulted in the intermediate compound **16** (Scheme 3). In the formation of compound **16**, there is a mechanistic possibility of getting two structural isomers, namely, N-9 isomer and N-7 isomer. Here,

https://dx.doi.org/10.1021/acs.jmedchem.0c00011
J. Med. Chem. 2020, 63, 4776−4789

Scheme 2[a]

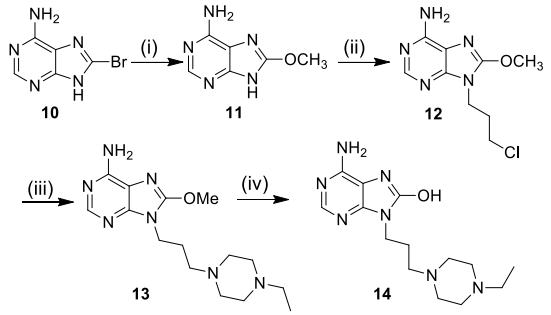

[a]Reagents and conditions: (i) 5 M solution of sodium methoxide in methanol (10 equiv), reflux, 12 h, 72%; (ii) 1-bromo-3-chloropropane (2.0 equiv), potassium carbonate (2.6 equiv), rt, 16 h, 78%; (iii) ethylpiperazine (3.0 equiv), potassium carbonate (1.5 equiv), rt, 6 h, 63%; (iv) 4 M HCl in 1,4-dioxane 3 h, 86%.

Scheme 3[a]

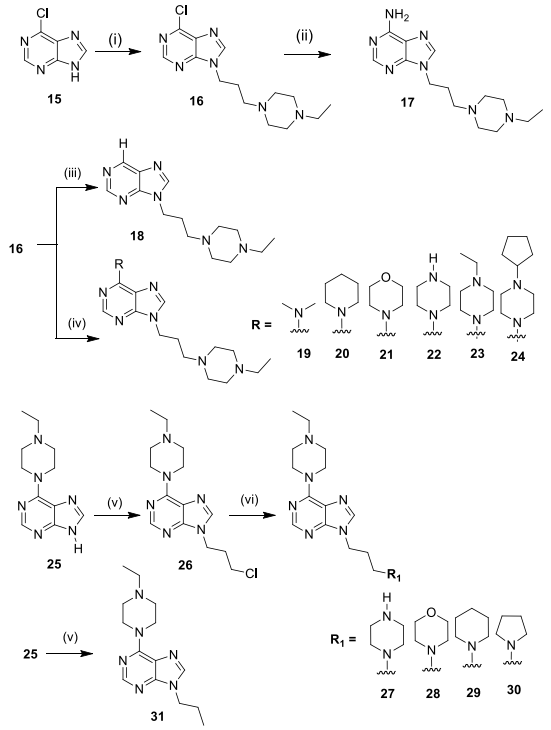

[a]Reagents and conditions: (i) 1-(3-chloropropyl)-4-ethylpiperazine (2.0 equiv), potassium carbonate (2.0 equiv), DMF, 60 °C, 12 h, 84%; (ii) ammonia in ethanol (7.0 equiv), 60 °C, 12 h, 67%; (iii) H_2, Pd/C, THF, rt, 2 h, 91%; (iv) respective amine, potassium carbonate (2.0 equiv), CH_3CN, reflux, 12 h, 73−95%; (v) 1-bromo-3-chloropropane for (**26**) and 3-bromopropane for (**31**) potassium carbonate (2.0 equiv), DMF, rt, 12 h, 71−78%; (vi) respective amine, potassium carbonate (2.0 equiv), DMF, 60 °C, 12 h, 78−93%.

we obtained exclusively N-9 isomer, and the structure was confirmed by the X-ray crystallographic structure of hydrochloride salt of intermediate compound **16** (Supporting Information, Figure S6). Thereafter, the chloride group at C-6 position was replaced by free $-NH_2$ group by treating with ammonia in ethanol at 60 °C to derive compound **17**. Reduction of the C-6 chloro group using palladium-carbon in **16** gave compound **18**. The chloro group at C-6 of intermediate **16** was substituted with different organic amines such as dimethylamine, piperidine, morpholine, piperazine, ethylpiperazine, and cyclopentylpiperazine to yield compounds **19**, **20**, **21**, **22**, **23**, and **24**, respectively. The N-9 position of **25** was treated with 1-bromo-3-chloropropane to get chloro intermediate **26**, which was subsequently reacted with various azacyclic bases such as piperazine, morpholine, piperidine, and pyrroline to yield compounds **27**, **28**, **29**, and **30** respectively. Compound **31** with propyl substitution at N-9 position was made from **25** using the same protocol used for the preparation of **26**. Structural conformation of compound **23** was made by the analysis of NOESY, HMBC spectra, the detail is in the Supporting Information.

RESULTS AND DISCUSSION

The importance of butoxy at C-2, $-NH_2$ at C-6 and hydroxyl at C-8 in TLR7-agonism by purine chemotypes is established.[38,39] We selected compound **7** as a starting point as it contains all the essential features of a TLR7 agonist. The synthetic strategy (Scheme 1) for compound **7** allowed us to readily introduce an additional basic center at N-9. Replacing piperidine with ethylpiperazine led to the enhancement in agonism in **9** (Scheme 1), which had an EC_{50} of 0.9 μM as opposed to 2.6 μM for **7** (Figure 1a,b, Table 1). Based on the previous SAR studies, it has been established that substituents such as butoxy at C-2 position are a key feature for TLR7 agonism.[23,25] As discussed before, we hypothesized that C-2 butoxy may be targeted to transform the potent TLR7 agonist **9** into a TLR7 antagonist. Indeed, the removal of C-2 butoxy in **14** (Scheme 2), led to the disappearance of TLR7 agonism and acquisition of considerable antagonism (Figure 1c,d, Table 1). Thus, we were able to identify a "chemical switch" at C-2 that could make a potent purine scaffold TLR7 agonist to loose agonistic properties and acquire antagonistic properties toward TLR7.

This novel purine scaffold molecule **14**, despite showing significant antagonism to human TLR7, had an IC_{50} (43.1 μM) too high for a therapeutically relevant antagonist. Therefore, we explored if omission of other essential agonist-specific molecular features from **14** can help to develop more potent antagonists with translational potential. We found that removal of the hydroxyl group at C-8 led to rather a loss of all activity against TLR7 in compound **17** at 50 μM. The importance of the $-NH_2$ group was evident from the crystal structure of guanosine as well as the chemical ligands from imidazoquinoline class too.[27] Also, the SAR study at C-6 position of purines has depicted the significance of $-NH_2$ group.[40] Accordingly, we focused on the modification at C-6 position. Neither complete deletion of the $-NH_2$ group from C-6 in compound **18** nor converting the $-NH_2$ at C-6 to dimethylamino in compound **19** brought antagonistic activity toward TLR7 (Table 1) at 50 μM. Next, we extended the dimethylamino group of compound **19** with different azacyclic moieties like piperidine, morpholine, and piperazine. Interestingly, piperidine substitution at C-6 position in compound **20** regained the TLR7 antagonistic effect, and the compound shows moderate TLR7 antagonism with an IC_{50} value of 23.9 μM. Replacement of piperidine with morpholine in compound **21** showed comparable TLR7 antagonism with an IC_{50} of 25 μM. Because morpholine cannot be further extended at 4′ position, we introduced piperazine in compound **22** with an aim for further derivatization, but the TLR7 antagonistic potency decreased to 39.3 μM. However, ethyl substitution on the piperazine NH group in compound **23** regained the TLR7

https://dx.doi.org/10.1021/acs.jmedchem.0c00011
J. Med. Chem. 2020, 63, 4776−4789

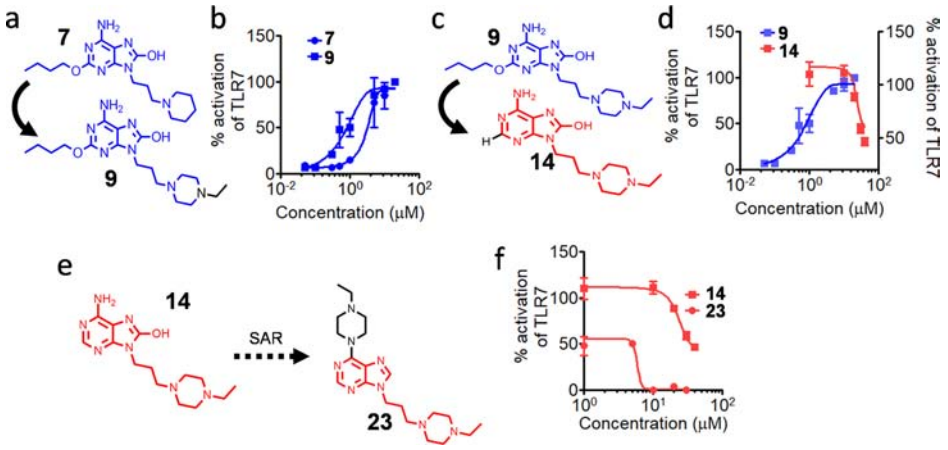

Figure 1. Discovery of TLR7 antagonist from known TLR7 agonist. (a,c,e) Conversion of TLR7 agonist **7** (EC_{50} = 2.6 μM) to a more potent TLR7 agonist **9** (EC_{50} = 0.9 μM) by the addition of ethylpiperazine group (a) compound **9** to weak TLR7 antagonist **14** (IC_{50} = 43.1 μM) by the elimination of butoxyl group (c) **3** to potent TLR7 antagonist **23** (IC_{50} = 4.7 μM) by systematic SAR study (e). (b,d,f) HEK-Blue TLR7 reporter cells were incubated overnight in the presence of indicated concentrations of given compounds and on the following day the culture supernatants were subjected to a colorimetric assay to measure the degree of TLR activation/inhibition. Data are represented as mean ± SEM.

Table 1. SAR Depicting the Conversion of Agonist to Antagonist

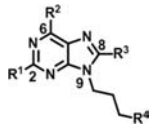

Comp. No.	R^1	R^2	R^3	R^4	TLR7 Agonism (μM) EC_{50}	TLR7 Antagonism (μM) IC_{50}
7	-OBu	$-NH_2$	-OH		2.6±0.05	a
9	-OBu	$-NH_2$	-OH		0.9±0.01	a
14	H	$-NH_2$	-OH		b	43.1±4.1
17	H	$-NH_2$	H		b	a
18	H	H	H		b	a
19	H	NMe_2	H		b	a
20	H		H		b	23.9±3.1
21	H		H		b	25.0±3.5
22	H		H		b	39.3±3.7
23	H		H		b	4.7±0.4
24	H		H		b	6.2±1.5
27	H		H		b	37%[c]
28	H		H		b	40.0±4.2
29	H		H		b	15.8±1.8
30	H		H		b	48.3±4.9
31	H		H	H	b	a
Hydroxychloroquine					NT	8.6±1.2

[a]No significant inhibition at 50 μM. [b]No significant activation at 50 μM. [c]% inhibition at 50 μM. NT-not tested. Hydroxychloroquine is a positive control.

antagonistic effect in single digit micromolar level with an IC_{50} value of 4.7 μM. Of note here, an ethylpiperazine group at N-9 led to enhancement of TLR7 agonism, while introducing the same group at C-6 potentiated TLR7 antagonism. Further logical extension of the ethyl group in compound **23** with more hydrophobic cyclopentane group in compound **24** led to slight decrease in the TLR7 antagonist activity (IC_{50} value of 6.2 μM, Table 1). Figure 1 is a snapshot of our SAR development depicting minimal structural requirements and a singular chemical switch that could transform a TLR7 agonist into a TLR7 antagonist in the same purine scaffold, which is represented in a TLR7 reporter assay done in parallel using an established TLR7 agonist (CL264), the purine agonists **7** and **9** as well as the TLR7 antagonist **23** which has been shown to inhibit CL264-induced TLR7 activation (Figure 1g).

Initially, in compound **9** it was observed that the introduction of weak base at N-9 can modulate TLR7 activity. Thus in our next development, we further explored the role of weak base at N-9 position with different groups such as morpholine, pyrrolidine, and piperidine. Replacing ethyl-

https://dx.doi.org/10.1021/acs.jmedchem.0c00011
J. Med. Chem. 2020, 63, 4776−4789

piperazine group in compound **23** with piperazine in **27** led to drastic fall in TLR7 antagonist activity (37% inhibition at 50 μM). The result suggests that the hydrophobic ethyl group is essential for TLR7 antagonistic activity. The result correlates well with our first set of SAR results where unsubstituted piperazine at C-6 in compound **22** showed 8 fold less potency than ethyl substituted piperazine group in **23**. Further substitution with morpholine, piperidine, and pyrrolidine yielded less potent TLR7 antagonist compound **28**, **29**, and **30** with IC_{50} 40.0, 15.8, 48.27 μM, respectively. Expectedly, elimination of weak base at N-9 in compound **31** led to complete loss of TLR7 antagonism at 50 μM (Table 1). To ensure the validity of TLR7 antagonism assay, the ability of different doses of hydroxychloroquine to inhibit TLR7 activation was studied as a positive control. Comparison between compound **17** with **23** suggests that introduction of ethylpiperazine group with an additional basic center and an extended hydrophobic attachment at C-6 had profound potentiating effect on TLR7 antagonism in purine scaffold, whereas additional basic center at N-9 can modulate the TLR7-targeted activity (either agonism as in **7** and **9**, or antagonism as in **23** and **29**).

None of the TLR7 antagonists showed any TLR7 agonism up to 50 μM dose (Supporting Information, Figure S2) which ruled out the possibility of partial agonism. As TLR7 and TLR8 show high degree of structural similarity,[19] next we monitored the efficacy of our TLR7 antagonists in TLR8 antagonistic assay, and we found that none of the TLR7 antagonists showed significant TLR8 inhibition (Supporting Information, Figure S3) up to 50 μM. The result strongly suggests that the TLR7 antagonists reported in the manuscript are selective for TLR7 when compared with TLR8 antagonism.[41] TLR7 antagonistic effect of compound **23** was further assessed by evaluating the ability of our compound to inhibit the production of TLR7-triggered proinflammatory cytokines such as IL-6 and TNFα.[41,42] Compound **23** showed 42.9% inhibition (Figure 2a) of IL-6 gene transcription at IC_{50} dose (5 μM) in HEK-Blue TLR7 cell line. Inhibition of proinflammatory cytokines was measured by real time polymerase chain reaction (RT-PCR) using selective TLR7 agonist CL264 as positive control. For further validation employing *ex vivo* human blood-derived model, we observed the inhibition of TLR7-driven TNFα induction in primary human peripheral blood mononuclear cells (hPBMCs) by ELISA (Figure 2b). These results led us to conclude that our compound of interest is a potent TLR7 antagonist capable of inhibiting TLR7-mediated immune responses as depicted by the inhibition of IL-6 and TNFα production in response to TLR7 activation. Thus, we have successfully identified hitherto unknown site-specific substitutions that can switch a well-established purine scaffold TLR7 agonist into a TLR7 antagonist, as demonstrated through the TLR7 reporter assay.

TLR7 and TLR8 share almost similar ligand binding domains. Both the TLRs have one small molecule ligand binding site and another ssRNA binding site.[27] Zhang *et al.*[19] reported a third binding site for the inhibition of TLR8 in the rest state. The binding model was extrapolated for finding new antagonist binding zone in TLR7. Karroum *et al.* validated this new antagonist binding site in TLR7 through systematic computational analysis of imidazo[1,2-*a*]pyrazines, imidazo-[1,5-*a*]quinoxalines, and pyrazolo[1,5-*a*]quinoxalines class TLR7 antagonists.[41] Because of the unavailability of the human TLR7 crystal structure, we have built homology model

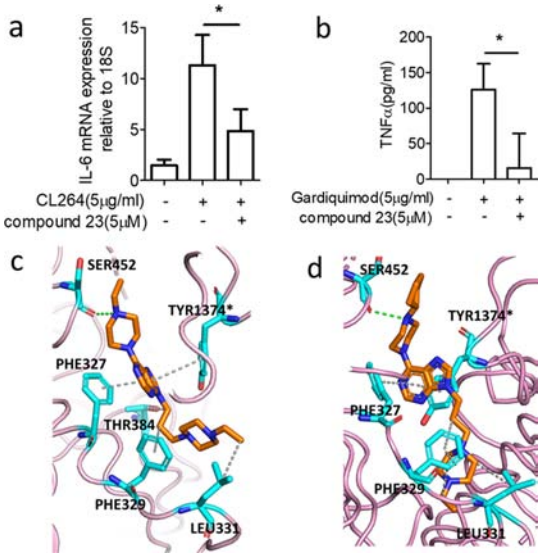

Figure 2. Inhibition of proinflammatory cytokines and docking study of compound **23** with homology modeled hTLR7 (a) HEK-Blue TLR7 reporter cells were treated with 5 μM compound **23**, 1 h prior to stimulation with CL264, 6 h after which, the cells were harvested and subjected to gene expression studies to monitor the mRNA levels of the IL6 gene relative to that of 18S (housekeeping gene) in the presence and absence of compound treatment. Data are represented as mean ± SEM, $*p < 0.05$, $n = 6$. Unpaired Student's *t*-test was done to measure statistical significance. (b) Primary hPBMCs were treated with 5 μM compound **23**, 1 h prior to stimulation with gardiquimod and incubated overnight. On the following day, the culture supernatants were subjected to ELISA to measure the degree of TLR activation/inhibition in terms of TNFα production. Data are represented as mean ± SEM, $*p < 0.05$, $n = 4$. Paired Student's *t*-test was done to measure statistical significance. (c) Interaction between TLR7 ectodomain (homology model template PDB ID: 5WYZ) and compound **23**. (d) Interaction between TLR7 ectodomain and compound **24**. Hydrogen bonds and hydrophobic interactions are shown by green dashed line and grey dashed line, respectively. *marks residues are in chain B.

structure of TLR7 (Supporting Information, Figure S7). Molecular docking study and validation was performed using Discovery Studio suite 4.1 (Supporting Information, Figure S8a), which shows that our TLR7 antagonists also bind in the same region, attaining similar pattern of interactions along with newer interactions (Figure 2c,d). The molecular docking indicates that the purine ring of the lead molecule **23** is sandwiched between two hydrophobic residues Phe329 and Tyr1374 forming $\pi-\pi$ stacking interactions (Figure 2c). Hydrogen bonding between the hydroxyl group of Ser452 with nitrogen of C-6 position of ethylpiperazine was observed in compound **23** as one of the key important interaction signifying the importance of terminal nitrogen in the piperazine group as observed in the structure−activity relationships between compounds **19**, **20**, and **21** with dimethylamino, piperidine, and morpholine groups, respectively. N-9 position of the alkyl linker with pendent hydrophobic amine was stabilized by the hydrophobic interaction of Leu331 and Phe329. The significance of the ethyl group can be observed by comparing the inhibitory potency of compounds **23** and **27**. Compound **23** showed IC_{50} value of 4.7 μM, whereas compound **27** without the ethyl group showed 37% inhibition at 50 μM. Similar binding interactions were observed for other potent TLR7 antagonist

https://dx.doi.org/10.1021/acs.jmedchem.0c00011
J. Med. Chem. 2020, 63, 4776−4789

Table 2. *In Vitro* Pharmacokinetics of Compound 23

				Caco-2 permeability P_{app} (10^{-6} cm/s)			plasma stability		microsomal stability			
									human		mice	
aq. sol μg/mL	clog *P*	PSA Å^2	NRB[a]	A → B[b]	B → A[c]	efflux ratio	human[d]	mice[d]	$T_{1/2}$ (min)	QH %	$T_{1/2}$ (min)	QH %
200.3	1.38	52.6	7	3.57	9.28	2.6	95%	99.2%	90.3	26.5	111.8	14.4

[a]Number of rotatable bolds. [b]Apical to basal. [c]Basal to apical. [d]Remaining after 2 h.

compound **24** (Figure 2d). From the molecular docking analysis of our other TLR7 antagonists, we can conclude that along with hydrogen bonding with Ser452, hydrophobic interactions play a vital role in determining TLR7 antagonism (Supporting Information, Figure S8).

Selectivity of TLR7 antagonist **23** over TLR8 can be anticipated through docking analysis. TLR8 and TLR7 share similar antagonistic binding sites except for one single residue change.[41] Polar residue Thr384 for TLR7 is replaced by nonpolar bulky Ile403 in TLR8. The molecular modeling of compound **23** in TLR7 indicates that the N-9 flexible linker is 5 Å away from Thr384 (Figure 2c). It can be anticipated that due to the steric bulk of Ile403 compound **23** is unable to bind to TLR8, which could be the probable reason for selectivity of our antagonists toward TLR7 over TLR8.

We selected compound **23** for further investigation. Initially we aimed at gathering insights about *in vitro* pharmacokinetics of **23** through a series of established assays. The aqueous solubility of **23** was found to be considerable (200 μg/mL) at pH 7.4, and calculated clog *P* value was 1.38 (Table 2). The polar surface area (52.6 Å^2) and seven rotatable bonds were also good indicators that compound **23** would have favorable oral bioavailability (Table 2).[43] On Caco-2 permeability assay, the efflux ratio of **23** was found to be 2.6, suggesting that this molecule would have moderate membrane permeability and is not likely to be a substrate for efflux transporters, *viz.* P-glycoprotein. In a nut shell, these results reflect that compound **23** may have good adsorption in the gastrointestinal tract. Compound **23** also showed acceptable plasma stability as well as metabolic stability (liver microsomal assay), assessed in case of both mice and human (Table 2). Moreover, compound **23** showed no cytotoxicity on HEK293 cells *in vitro* up to a concentration of 100 μM (Figure S4).

Finally, to assess *in vivo* applicability of this novel TLR7 antagonist **23**, we checked the *in vivo* pharmacokinetics of the molecule on oral and intravenous administration to C57BL/6 mice in two doses of 10 mg/kg and 15 mg/kg. The maximum plasma concentration (C_{max}) surpassed the *in vitro* IC_{50} against TLR7 in 15 mg/kg oral dose whereas in 10 mg/kg dose C_{max} remained below the IC_{50}. It was found that compound **23** was rapidly absorbed into body (Figure 3a) with a half-life of 4.6 h upon 15 mg/kg oral dose (Figure 3c). As compound **23** is basic in nature, it shows good Vss (4.2 L/kg, Figure 2c) which reflect the high duration of drug in target site.[44] Finally, all of the favorable range of *in vitro* and *in vivo* pharmacokinetics (Figure 3) of compound **23** adds up to give excellent oral bioavailability (F = 70.8%, Figure 3a,b).

To validate *in vivo* efficacy of **23** for TLR7 antagonism in a clinically relevant context, we utilized an established preclinical model of the cutaneous autoimmune disease psoriasis. Daily application of the TLR7 agonist imiquimod to the skin of C57BL/6 mice leads to a psoriasiform inflammation in 6 days, which closely mimics the human disease in terms of morphology, histopathology, and the underlying immunocellular involvements.[15] This preclinical model has not only been the key support for the pathogenetic role of TLR7 in this clinical context but also has been instrumental for discovery of other downstream pathogenetic mechanisms for the disease as well as validation of most of the clinically used targeted biologic therapies used clinically.[45] We administered 15 mg/kg body weight compound **23** by oral gavage to the mice daily from the first day of application of imiquimod cream and on the 6th day assessed disease development, in comparison with vehicle-administered control mice having developed imiquimod-driven psoriasis (Figure 4a). We found that oral administration of our TLR7 antagonist **23** could totally prevent the cutaneous pathology in terms of macroscopic morphology (Figure 4b). There was also significant retardation in skin thickening in the antagonist-treated mice (Figure 4c).

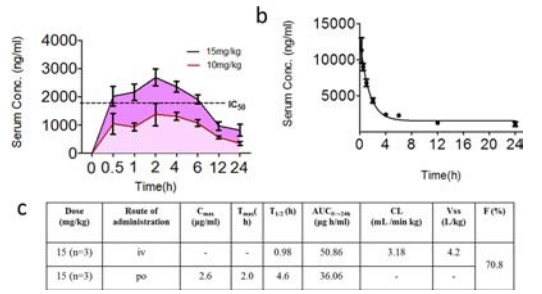

Figure 3. Pharmacokinetics profiling of potent TLR7 antagonist **23**. (a) Doses of 15 mg/kg and 10 mg/kg body weight of compound **23** was orally administered to 3 sets of male C57BL/6 mice. (b) Dose of 15 mg/kg body weight of compound **23** was intravenously administered to 3 male C57BL/6 mice. (c) Calculated pharmacokinetics parameter in tabulated formed. 2% ethanol in PBS (0.01 M, pH = 7.4) buffer used as vehicle. The concentration of compound present in serum at indicated time points was quantified by LC−MS/MS (Figure S4).

Histopathologic scoring of the lesional skin in the treated mice revealed nearly complete absence of the pathognomonic features like hyperkeratosis, parakeratosis, acanthosis, spongiosis, papillomatosis, suprapapillary thinning, vascular dilatation, microabscesses and pustule formation (Figure 5a,b). On scoring the histopathology based on the listed features (Figure 5c), there was total amelioration of disease on oral administration **23** (Figure 5d,e).

In a repeat experiment too, the amelioration of cutaneous pathology with compound **23** was evident in terms of reduction in skin fold thickness (Figure S5) as well as in terms of reduction in the tissue expression of the proinflammatory cytokine TNFα (widely implicated in the pathogenesis of psoriasis) and four major type I IFN signature genes (ISGs) MX1, MX2, ISG15, and IFIT1 (surrogate markers for type I IFN induction *in situ*) (Figure 6a−e).

Moreover, histomorphology of lung, liver, and kidney did not show any remarkable pathologic changes following oral administration of compound **23** for 7 consecutive days at a

https://dx.doi.org/10.1021/acs.jmedchem.0c00011
J. Med. Chem. 2020, 63, 4776−4789

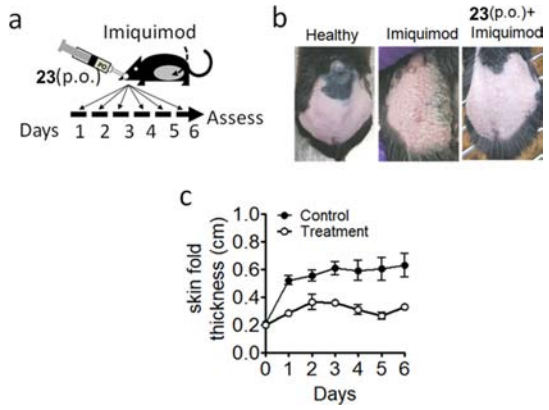

Figure 4. Efficacy of TLR7 antagonist in rodent psoriasis model. (a) Schematic representation of experimental protocol followed—compound **23** or vehicle was orally administered for 7 consecutive days starting one day before (day 0) topical application of imiquimod on the dorsal skin surface, which was done for 6 consecutive days. The following day mice were sacrificed, normal and psoriatic skin harvested and subjected to histopathological evaluation. (b) (Left) Shaved normal dorsal skin before imiquimod application, (middle) shaved imiquimod treated dorsal skin of vehicle treated mouse on day 7 showing significant scale formation on skin, and (right) shaved imiquimod treated dorsal skin of compound **23** treated mouse on day 7 showing markedly lesser scale formation compared to previous group. (c) Thickness of skin fold of vehicle-treated mice (n = 9) and compound-treated mice (n = 9) were recorded and plotted every day (3 readings each) to monitor the gradual changes taking place upon daily imiquimod application. Data are represented as mean ± SEM. 2% ethanol in PBS (0.01 M, pH = 7.4) buffer was used as vehicle.

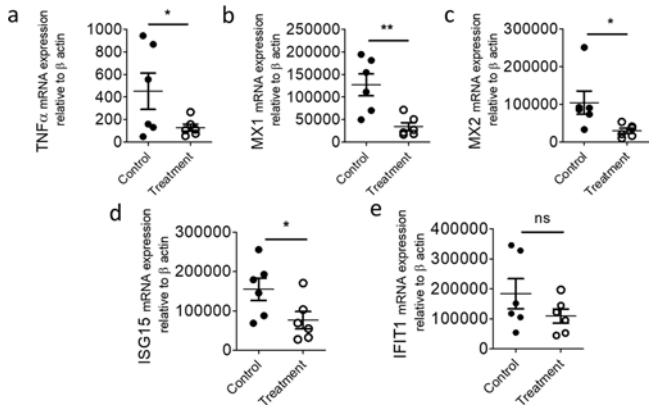

Figure 6. Inhibition of pro-inflammatory TLR7-mediated gene expression in rodent model of psoriasis. (a–e) Dorsal skin sections obtained from C57BL/6 mice treated with vehicle (n = 6) or treated with 15 mg/kg compound **23** (n = 6) for 7 consecutive days were processed and subjected to gene expression studies to measure expression of indicated genes—TNFα (a), MX1 (b), MX2 (c), ISG15, (d) and IFIT1 (e). (*p < 0.05, **p < 0.01, ns = nonsignificant).

dose rate of 15 mg/kg as compared to vehicle administration (Figure 7). No notable toxicity-induced pathology was discernible, *viz.* changes in parenchymal architecture of the liver, hepatocyte survival, fatty infiltration, or inflammation in compound treated mice as compared to vehicle treated mice (Figure 7a,b). Similarly, no discernible changes were observed in lung microanatomy as well. No evidence of immune

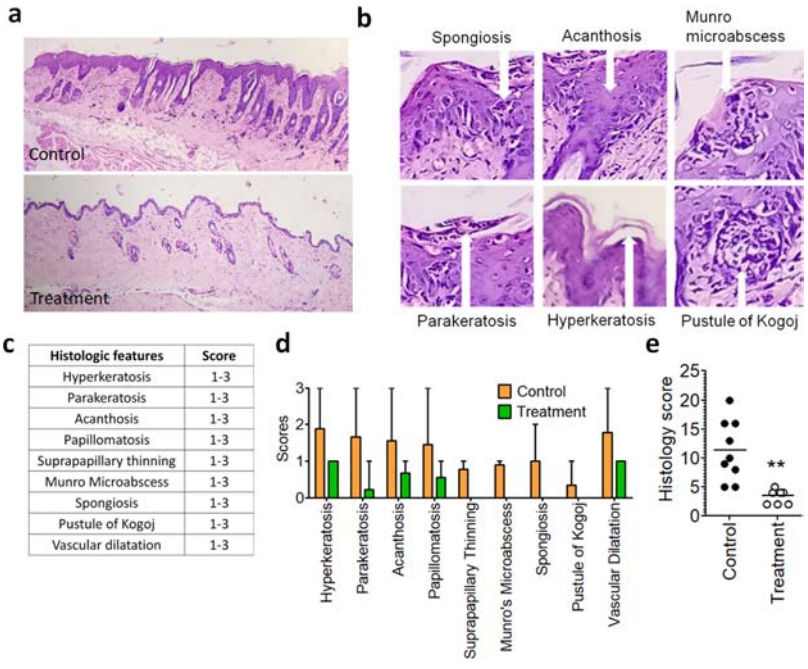

Histologic features	Score
Hyperkeratosis	1-3
Parakeratosis	1-3
Acanthosis	1-3
Papillomatosis	1-3
Suprapapillary thinning	1-3
Munro Microabscess	1-3
Spongiosis	1-3
Pustule of Kogoj	1-3
Vascular dilatation	1-3

Figure 5. Histopathologic scoring of the H&E-stained skin sections of mice with psoriatic disease. (a) (Upper) H&E stained, imiquimod exposed, dorsal skin section of vehicle-treated mouse showing marked thickening of epidermis and presence of hyperkeratosis, papillomatosis, and acanthosis, (lower) H&E stained, imiquimod exposed, dorsal skin section of compound **23** treated mouse showing appreciably lesser thickening of epidermis. (b) Representative images showing the key pathognomonic histopathologic features used for scoring. (c) All histological features were scored based on their severity and preponderance, 1 being least severe and 3 being most severe. (d) Imiquimod exposed dorsal skin sections from compound-treated or vehicle-treated mice were graded on the basis of different clinically relevant histopathological parameters such as hyperkeratosis, acanthosis, papillomatosis, suprapapillary thinning, Munro's microabscess, spongiosis, pustule of Kogoj, vascular dilatation of control group (n = 9), and compound-treated group (n = 9), as a measure of disease severity. (e) Data on scores for individual pathognomonic features compared between control and treatment groups. (**p < 0.01).

https://dx.doi.org/10.1021/acs.jmedchem.0c00011
J. Med. Chem. 2020, 63, 4776–4789

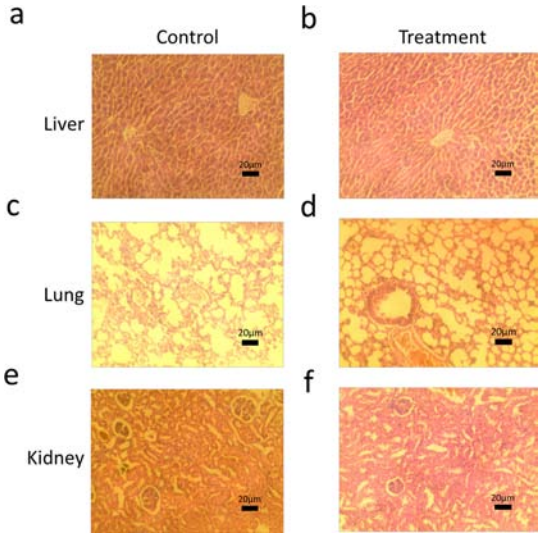

Figure 7. Short-term visceral toxicity assessment. (a–f) Representative images of H&E stained sections of liver specimens (a,b), lung specimens (c,d), and kidney specimens (e,f) obtained from C57BL/6 mice treated with vehicle (a,c,e) or 15 mg/kg compound **23** (b,d,f) for 7 consecutive days.

infiltration or alveolar architecture was observed in the lungs (Figure 7c,d). In kidneys, no glomerular hypertrophy, mesangial proliferation, capsular space obliteration, or inflammation was observed in the compound-treated mice as compared to control mice (Figure 7e,f). We also did not observe any behavioral or physiological abnormalities in experimental animals within the study period, thus indicating that oral administration of compound **23** does not cause any apparent short-term visceral cytotoxity in C57BL/6 mice. Thus, this novel TLR7 antagonist **23** was very efficient in preventing a TLR7-driven TNFα and type I IFN induction and the autoimmune pathology *in vivo*.

CONCLUSIONS

In summary, we have been able to define minimal structural requirements in a purine scaffold TLR7 agonist **1** and identify a singular "chemical switch" in the scaffold that could transform the molecule to a TLR7 antagonist. We established that a small structural modification in TLR7 ligand can lead to reversal in their functional activity. We further developed on that and could design a potent TLR7 antagonist **23**, which had favorable *in vitro* and *in vivo* pharmacokinetics with excellent oral bioavailability (70.8%) in mice. Interestingly, the ethylpiperazine group at N-9 led to enhancement of TLR7 agonism, while introducing the same at C-6 led to potentiation of TLR7 antagonism. Introduction of an additional basic center at C-6 has a profound potentiating effect on TLR7 antagonism in purine scaffold. Our SAR studies successfully identified site-specific substitutions that can switch a well-established purine scaffold TLR7 agonist into TLR7 antagonist. None of the TLR7 antagonist showed any TLR7 agonism, which signifies that they are pure antagonists. It is worthwhile to mention that all the TLR7 antagonists reported herein showed excellent selectivity against TLR8. The docking analysis of our TLR7 antagonists showed that the purine ring is sandwiched between two hydrophobic residues Phe329 and Tyr1374 forming $\pi-\pi$ stacking interactions along with hydrogen bonding with Ser452, which plays a vital role in determining TLR7 antagonism. Finally, we could validate the *in vivo* efficacy of this TLR7 antagonist in a clinically relevant murine model of psoriasis. The histomorphology of lung, liver, and kidney did not show any remarkable pathologic changes following oral administration. The TLR7 antagonist **23** thus appears to be a very promising lead molecule for further development into clinically translatable TLR7 antagonists that can be first-in-class therapeutic agents in the relevant clinical contexts, which include a number of autoimmune diseases accounting for significant morbidity worldwide.

EXPERIMENTAL SECTION

Aqueous Solubility Assay. Dimethyl sulfoxide (DMSO, 6 μL, 50 mM) stock was added to the deep well plate containing 594 μL of pH 7.4 0.25 M phosphate buffer (including DMSO control), mixed, and incubated for 18 h at room temperature (rt) with constant mixing at 300 rpm. The plate was sealed well during the incubation process. After incubation, the samples were centrifuged for 20 min at 4000 rpm. The supernatant (400 μL) was analyzed by high-performance liquid chromatography (HPLC)-UV. The DMSO content in the sample was 1.0%, and the final concentration of the compound in deep-well plate was 500 μM. The spectrum was read using a Shimadzu UV spectrophotometer at 240 nm (Calculation is in Table S1).

Caco-2 Permeability Assay. Stock (10 mM) of compound in DMSO was diluted with Hank's balanced salt solution (HBSS) buffer pH 7.4 to a final concentration of 10 μM. For the proliferation of cells, 250 μL of Dulbecco's modified Eagle medium (DMEM) was added to the basal compartment of 96-well multiscreen Caco-2 plate and seeded 12,000 cells/well (0.16 × 106 cells/mL) in all of the apical wells placed in a CO_2 incubator at 37 °C. On the day of assay, the medium was removed and washed twice with HBSS buffer. HBSS buffer (250 μL) with 2% bovine serum albumin (BSA) was added to basal wells and 75 μL of the test compound was added to apical wells. Basal samples (25 μL) were collected at 120 min and processed as mentioned below. The test compound (250 μL) and 75 μL of HBSS buffer with 2% BSA was added to basal wells and apical wells, respectively. At 120 min, 25 μL of apical samples was collected and processed as stated below. A single-point calibration curve in HBSS buffer with 2% BSA was used. Donor samples and receiver samples were diluted 1:1 with HBSS separately while the former contains 2% BSA. It was precipitated with 200 μL of acetonitrile containing internal standard and vortexed for 5 min @ 1000 rpm, and centrifuged at 4000 rpm for 10 min. Finally, 100 μL of the supernatant was diluted with 200 μL of water and submitted for liquid chromatography–mass spectrometry (LC–MS)/MS analysis. (Calculation is in Table S2).

Plasma Stability Assay. Stock (25 μM) of test compound was prepared in acetonitrile from the stock solution of 10 mM in DMSO. By diluting acetonitrile/water (50:50) from the previously prepared 10 mM stock, 125 μM sample of 200 μL was prepared. For 0 min samples, plasma was heat inactivated at 56 °C for 45 min and to it 3 μL of 25 μM test compound was added to make the final volume 75 μL. In 200 μL acetonitrile, a 25 μL aliquot of the mixture was taken and crashed. At 0, 15, 30, 60, and 120 min, a 25 μL aliquot of the sample was precipitated immediately with 200 μL of acetonitrile, centrifuged at 4000× relative centrifugal force (RCF), 4 °C for 20 min and analyzed on LC–MS/MS (Calculation for human plasma stability in Table S3 and mice plasma stability Table S4).

Microsomal Stability. Stock (10 mM) of test compound in DMSO was diluted with 1:1 water acetonitrile to get 200 μL 1 mM stock solution. Working concentration (100 μM) of test compound was prepared by diluting 1 mM stock solution of test compound in DMSO with acetonitrile: water (1:1). Nicotinamide adenine dinucleotide phosphate (NADPH) cofactor solution (2.5 mM) was prepared from 16 mM stock solution and 3.33 mg/mL working stock of liver microsomes was prepared from 20 mg/mL liver microsome master stock solution. Phosphate buffer (85 μL) of pH 7.4 was mixed

https://dx.doi.org/10.1021/acs.jmedchem.0c00011
J. Med. Chem. 2020, 63, 4776–4789

with 2.5 μL of test compound (100 μM) and 75 μL 3.33 mg/mL HLM in a deep well plate for preincubation of 10 min at 37 °C. The mixture (32.5 μL) was added to 17.5 μL buffer and incubated for 60 min without NADPH cofactor. For 0 min sample, 16.5 μL of the preincubated mixture was crashed with 200 μL of acetonitrile and 8.75 μL of cofactor was added to it. 62 μL NADPH-cofactor was added to remaining incubation mixture and kept for 60 min at 37 °C. For other time point samples, 25 μL of incubation mixture at 5, 10, 30, 60, and 60 min without cofactor was precipitated immediately with 200 μL of acetonitrile containing internal standard and vortex for 5 min at 1200 rpm. The samples were centrifuged at 4000× RCF, 4 °C for 10 min. The supernatant (150 μL) was diluted with 150 μL of water and analyzed on LC−MS/MS (calculation for human microsomal stability in Table S5 and mice microsomal stability Table S6).

TLR7 Agonism and Antagonism Assay Using HEK-Blue hTLR7 Reporter Cell Line. The TLR7 agonistic or antagonist activity of synthesized compounds was assayed using a HEK293 cell line engineered to express human TLR7 as well as a NF-κB induced SEAP. The assay was based on the principle that TLR activation with TLR agonist leads to downstream NF-κB activation which in turn induces SEAP production and secretion into culture supernatant, causing color change upon interaction with the detection media. 7×10^4 cells/well were seeded in 100 mg/mL Normocin supplemented complete DMEM medium and allowed to adhere to the substrate for 5 h at 37 °C and 5% CO_2. For antagonism assays, CL264 (TLR7 agonist, 5 μg/mL) was added to the cells preincubated for 1 h with indicated doses of compounds, whereas for agonism assays, cells were only treated with indicated doses of compounds. Following overnight incubation, 50 μL of culture supernatant from each well was added to 200 μL of QUANTI-Blue detection media and constantly monitored for color change. After 1−2 h of incubation, spectrophotometric reading at 655 nm wavelength was recorded. To ensure the validity of TLR7 antagonism assay, the ability of different doses of hydroxychloroquine to inhibit TLR7 activation was studied as a positive control. Two-tailed paired Student's *t*-test was performed using GraphPad Prism software version 5.0. HEK-Blue hTLR7 reporter cell line, Normocin, and CL264 were purchased from Invivogen, USA.

TLR8 Antagonism Assay Using HEK-Blue hTLR8 Reporter Cell Line. To ensure the specificity of the synthesized antagonists for human TLR7 and exclude the possibility of nonspecific antagonism toward human TLR8 which is structurally very similar to human TLR7, we performed reporter assays using HEK-Blue hTLR8 reporter cell line. The protocol used to perform this experiment was exactly same as that for the antagonism assay in HEK-TLR7 cell line, described above. The only difference was the usage of a TLR8 specific agonist CL075 (3 μg/mL) as the stimulant.

Cytotoxicity Assay in HEK293 Cell Line. 1, 5, 10, 20, 40, 60, 80, and 100 μM of indicated compounds were added to 6×10^4 HEK293 cells cultured incomplete DMEM at 37 °C and 5% CO_2 overnight, following which cells were harvested in phosphate-buffered saline (PBS) (0.01 M, pH = 7.4), stained with 2.5 mg/mL PI for 1 min, and percentage of cells showing PI uptake in a flow cytometer (BD LSRFortessa) was measured.

IL-6 mRNA Expression Measurement through RT-PCR Analysis. HEK-Blue TLR7 cells were seeded in a 96-well plate at a density of 1×10^5 cells/well and allowed to attach overnight. Next morning, cells were preincubated with 5 μM of compound **23** for 1 h before being stimulated with 5 μg/mL of TLR7 agonist-CL264 for 6 h, following which cells were harvested in the TRIzol reagent (Invitrogen). Total RNA was isolated using the manufacturer's protocol followed by cDNA preparation using the Applied Biosystems kit, and RT-PCR was done using Bio-Rad SYBR Green Master Mix to measure the expression levels of IL6 gene relative to that of 18S (housekeeping gene). Primer sequences used, Hu-18S: forward: 5′-GTTGGTTTTCGGAACTGAGG-3′ reverse: 5′-TCGTTTATGGTCGGAACTACG-3′ and Hu-IL6: forward: 5′-CACAGACAGCCACTCACCTCTTC-3′ reverse: 5′-TTTGCTGCTTTCACACATGTTACTC-3′.

TLR7 Antagonism Assay in Primary hPBMCs. Primary hPBMCs were isolated from blood taken from healthy individuals after obtaining their informed consent as well as ethical approval from the Institutional Ethics Committee, in accordance with the guidelines mentioned in the Declaration of Helsinki. PBMCs were obtained by performing density gradient centrifugation and seeded at a density of 2×10^5 cells/well in a 96-well plate. PBMCs were preincubated with 5 μM of compound **23** for 1 h before being stimulated with 5 μg/mL of TLR7 agonist-gardiquimod overnight. Next day, the culture supernatant was collected and subjected to TNFα ELISA according to the protocol outlined by the manufacturer (Mabtech).

Homology Modeling and Docking Study. Homology structure of human TLR7 ectodomain was built using sequence Q9NYK1 retrieve from UNIPROT. The homology model structure of hTLR7 was built using TLR8 (PDB 5WYZ) as a template in discovery studio modeler suite, according to the reported procedure.[41] The docking experiment was performed using Discover Studio 4.1 C-DOCKER module. The docking method was optimized by analyzing reported TLR7 antagonist binding pose. Random conformers of compounds were searched using dynamics of 1000 steps. Docking simulation was performed using default parameter of C-DOCKER module in Discover Studio 4.1. The docked results were fully minimized using CHARMM force field with conjugate gradient 1.0. Pictorial view of docking pose was made using PyMOL.

***In Vivo* Pharmacokinetics and Bioavailability Study.** Nine 8−10 week old male C57BL/6 mice were recruited for the experiment. They were divided into three groups each having three mice. The compound was reconstituted in 2% ethanol in PBS (0.01 M, pH = 7.4). The mice belonging to the first group were given oral gavage with 15 mg/kg compound, the mice belonging to the second group were given oral gavage with 10 mg/kg compound, and the mice belonging to the third group were given intravenous injections of 15 mg/kg compound. Blood samples were drawn at 0, 0.5, 1, 2, 4, 6, 12, and 24 h after compound administration, and serum was isolated for the mice administered orally with the compound. On the other hand, blood samples were drawn at 0, 0.25, 0.5, 1, 2, 4, 6, 12, and 24 h after compound administration, and serum was isolated from the mice injected intravenously with the compound. 10 μL of serum from each mouse was extracted with 30 μL of LC/MS-grade acetonitrile + 0.1% formic acid (J.T. Baker) by alternate vortexing and chilling. Next, the supernatant was collected by centrifugation at 14,000 rpm for 10 min and analyzed by LC−MS/MS to measure the concentration of compound **23** in serum. Standards of compound **23** ranging from 74.688 to 5975 pg was prepared in serum and extracted in acetonitrile + 0.1% formic acid. MS was carried out in LTQ ORBITRAP XL using Hypersil Gold C18 column having a diameter of 100 × 2.1 mm with particle size being 1.9 μm. The column formed the stationary phase and a mixture of solution A (acetonitrile + 0.1% formic acid) and solution B (HPLC grade H_2O + 0.1% formic acid) formed the mobile phase. LC (injection volume 2 μL) was done using an isocratic solution containing 40% acetonitrile and 0.1% formic acid. The intact compound had a retention time of 0.76 min and (m/z) of 387.2988, while (m/z) of fragmented compound after MS/MS was 273.1852. All data were analyzed using the Thermo Xcalibur software.

***In Vivo* Efficacy Study.** Eighteen wild-type C57BL/6 male mice aged 8−10 weeks, provided by CSIR-IICB animal house facility, were divided into two groups; (1) control group-containing nine mice with induced psoriasis, treated with 2% ethanol in sterile PBS (0.01 M, pH = 7.4) (vehicle) and (2) treatment group-containing nine mice with induced psoriasis treated with compound **23**. Psoriasis was induced by daily topical application of 62.5 mg 5% w/w imiquimod cream (Imiquad; Glenmark, India) on a patch of shaved dorsal skin of the mice for 6 consecutive days. Vehicle and compound (15 mg/kg) were administered orally daily for 7 days, beginning 1 day prior to the start of imiquimod application. Skin fold measurement of the affected area was performed by a person blind to the experimental details and outcomes, with a standard Vernier caliper on a daily basis starting prior to imiquimod application and continuing till the end of the experiment. The experimental animals were sacrificed on the 7th day of imiquimod application, and portions of affected skin as well as

https://dx.doi.org/10.1021/acs.jmedchem.0c00011
J. Med. Chem. 2020, 63, 4776−4789

normal skin were collected from each animal (in 4% paraformaldehyde) for histopathological evaluation by hematoxylin and eosin (H&E) staining. All animal handling and mouse experiments were conducted in accordance with national and international guidelines and upon approval from the institutional ethics committee. All recommendations enlisted in the ACS Ethical Guidelines were followed while performing the mouse experiments.

RNA Isolation, cDNA Preparation, and Quantitative PCR. Lesional skin tissue derived from six control C57BL/6 mice and six compound **23** (15 mg/kg)-treated mice, following 7 consecutive days of oral administration (according to a protocol identical to that described in *in vivo* efficacy study), was minced into tiny pieces, frozen in liquid nitrogen, crushed using a mortar & pestle in TRIzol reagent (Invitrogen) and RNA was isolated according to the manufacturer's protocol. cDNA was produced using the high-capacity cDNA reverse transcription kit (Applied Biosystems). qPCR was performed to study the expression of the specified genes using SYBR Green Master Mix (Bio-Rad) (normalization was done with respect to the expression of β-actin—housekeeping gene).

Primer Sequences.

Mu-β actin	F: 5′-GAGGTATCCTGACCCTGAAGTA-3′
	R: 5′-GCTCGAAGTCTAGAGCAACATAG-3′
Mu-TNFα	F: 5′-AATGGCCTCCCTCTCATCAGTT-3′
	R: 5′-CCACTTGGTGGTTTGCTACGA-3′
Mu-MX1	F: 5′-TTCAAGGATCACTCATACTTCAGC-3′
	R: 5′-GGGAGGTGAGCTCCTCAGT-3′
Mu-MX2	F: 5′-TTCCAGCATCTGAATGCCTAC-3′
	R: 5′-ACTGGATGATCAAGGGAACG-3′
Mu-ISG15	F: 5′-ACGGTCTTACCCTTTCCAGTC-3′
	R: 5′-CCCCTTTCGTTCCTCACCAG-3′
Mu-IFIT	F: 5′-AGGCTGGAGTGTGCTGAGAT-3′
	R: 5′-TCTGGATTTAACCGGACAGC-3′

Short-Term *In Vivo* Toxicity Studies. Lung, liver, and kidney specimens of mice, following oral administration of compound **23** and vehicle for 7 consecutive days at a dose rate of 15 mg/kg, were collected and preserved in 10% formalin. H&E staining of tissue sections was performed for histomorphological evaluation. Images were acquired in an Olympus CKX41 brightfield inverted microscope at an objective magnification of 10× and monitored to study histomorphological parameters to deduce the visceral toxicity associated with compound **23** administration.

Chemical Synthesis and Methods. *General Methods.* All starting materials, reagents, and solvents were purchased from commercial suppliers and used without further purification. Air-sensitive reactions were carried out under a dry nitrogen or argon atmosphere. For thin-layer chromatography (TLC) on silica gel plates (Merck silica gel 60, F254) was used. RediSep Rf silica gel columns was used for column chromatographic purification on the Teledyne ISCO CombiFlash Rf system using 230−400 mesh silica gel. ^{1}H NMR was recorded at 300 MHz (Bruker-DPX), 400 MHz (Jeol), and 600 MHz (Bruker-Avance) frequency and ^{13}C NMR spectra were recorded at 75 MHz (Bruker-DPX), 100 MHz (Jeol), and 150 MHz (Bruker-Avance) using TMS as the internal standard. High-resolution mass spectra, HRMS (m/z), were measured using EI (Jeol-JMS 700 mass spectrometer), ESI (Q-Tof Micro mass spectrometer) techniques, and ESI (LTQ Orbitrap XL mass spectrometer). The purity of all the compounds was determined to be >95%, analyzed by Hitachi HPLC using column Xtimate C18 (4.6 mm × 150 mm, 5.0 μm) using gradient elution of acetonitrile in water 0−90% for 12 min and flow rate 1 mL/min with detection at 254 nm wavelength.

Synthesis of 2-Butoxy-9-(tetrahydro-2*H*-pyran-2-yl)-9*H*-purin-6-amine (2).[31] Sodium *t*-butoxide (0.8 g, 7.8 mmol) was added portion wise to the solution of 6 mL of *n*-BuOH and compound **1** (0.5 g, 2.0 mmol) in rt. The reaction mixture was then stirred for 12 h at 100 °C and concentrated under vacuum. Reaction mixture was purified by column chromatography to obtain pure compound **2** as yellowish liquid (77%). ^{1}H NMR (300 MHz, $CDCl_3$): δ 7.78 (s, 1H), 6.51 (s, 2H), 5.54 (dd, J = 2.4, 9.0 Hz, 1H), 4.23 (t, J = 6.6 Hz, 2H), 4.04 (d, J = 12.6 Hz, 1H), 3.69−3.61 (m, 1H), 1.99−1.88 (m, 3H), 1.72−1.59 (m, 4H), 1.44−1.36 (m, 2H), 1.14−1.09 (m, 1H), 0.87 (t, J = 7.2 Hz, 3H). ^{13}C NMR (100 MHz, $CDCl_3$): δ 162.3, 156.6, 151.0, 136.6, 115.5, 81.4, 68.6, 67.0, 31.7, 31.1, 24.9, 22.9, 19.3, 13.9. HRMS (ESI) m/z: (M + H) calcd for $C_{14}H_{22}N_5O_2$, 292.1773; found, 292.1766.

Synthesis of 2-Butoxy-8-methoxy-9-(tetrahydro-2*H*-pyran-2-yl)-9*H*-purin-6-amine (3). *N*-Bromosuccinimide (0.06 g, 0.36 mmol) was added to the solution of compound **2** (0.1 g, 0.3 mmol) in 0.6 mL $CHCl_3$ at 0 °C. Reaction was allowed to warm rt and stirred for 4 h at rt. The reaction mixture was diluted with $CHCl_3$ and washed with sodium thiosulfate. Evaporation of the $CHCl_3$ layer gave TLC wise pure bromo-substituted compound, and the next step was forwarded without further purification. This bromo derivative was refluxed with a 5 M solution of sodium methoxide in methanol (2.7 equiv) for 4 h, and the reaction mixture was concentrated under vacuum. The reaction mixture was then purified by column chromatography to give pure compound **3** as brownish semisolid (80%).^{1}H NMR (300 MHz, $CDCl_3$): δ 5.54 (dd, J = 1.8, 11.1 Hz, 1H), 5.28 (s, 2H), 4.28 (t, J = 6.6 Hz, 2H), 4.17−4.12 (m, 4H), 3.73−3.65 (m, 1H), 2.84−2.72 (m, 1H), 2.06−2.02 (m, 1H), 1.79−1.63 (m, 6H), 1.58−1.46 (m, 3H), 0.97 (t, J = 7.5 Hz, 3H). ^{13}C NMR (100 MHz, $CDCl_3$): δ 160.7, 154.3, 153.9, 151.5, 110.9, 81.3, 68.9, 66.9, 56.9, 31.2, 28.6, 24.9, 23.5, 19.3, 13.9. HRMS (ESI) m/z: (M + H) calcd for $C_{15}H_{24}N_5O_3$, 322.1879; found, 322.1884.

Synthesis of 2-Butoxy-8-methoxy-9*H*-purin-6-amine (4). Compound **3** (0.2 g, 0.5 mmol) was added to 1 mL solution of 10% TFA in methanol and stirred for 72 h. Completion of reaction was monitored by TLC and white precipitation was obtained after dilution of reaction mixture with ethyl acetate. Precipitation was filtered to obtain pure compound **4** as TFA salt (73%). ^{1}H NMR (300 MHz, $CDCl_3$ + 1 drop CD_3OD): δ 4.34 (t, J = 6.6 Hz, 2H), 4.05 (s, 3H), 1.74−1.64 (m, 2H), 1.41−1.33 (m, 2H), 0.88 (t, J = 7.5 Hz, 3H). HRMS (ESI) m/z: (M + H) calcd for $C_{10}H_{26}N_5O_2$, 238.1304; found, 238.1311.

General Procedure A for Synthesis of 2-Butoxy-9-(3-chloropropyl)-8-methoxy-9*H*-purin-6-amine (5). Compound **4** (0.1 g, 0.5 mmol) and potassium carbonate (0.2 g, 1.5 mmol) were dissolved in 1 mL of dimethylformamide (DMF), and the reaction mixture was heated at 50 °C for 2 h. 1-Bromo-3-chloropropane was added to the reaction mixture at rt and stirred for 16 h. The solvent was then removed, and the reaction was partitioned between $CHCl_3$ and water. Organic layer was then dried, and column chromatography was performed to get pure compound **5** as white solid (67%, mp 115 °C). ^{1}H NMR (300 MHz, $CDCl_3$): δ 5.32 (s, 2H), 4.26 (t, J = 6.6 Hz, 2H), 4.11−4.06 (m, 5H), 3.52 (t, J = 6.6 Hz, 2H), 2.28−2.20 (m, 2H), 1.77−1.70 (m, 2H), 1.51−1.44 (m, 2H), 0.95 (t, J = 7.2 Hz, 3H). ^{13}C NMR (100 MHz, $CDCl_3$): δ 160.8, 154.6, 153.8, 151.9, 110.9, 67.0, 56.8, 41.8, 38.7, 32.0, 31.2, 19.3, 13.9. HRMS (ESI) m/z: (M + H) calcd for $C_{13}H_{21}N_5O_2Cl$, 314.1384; found, 314.1387.

General Procedure B for Synthesis of 2-Butoxy-8-methoxy-9-(3-(piperidin-1-yl)propyl)-9*H*-purin-6-amine (6). Compound **5** (0.1 g, 0.3 mmol), potassium carbonate (0.1 g, 0.7 mmol), and piperidine (0.1 mL, 1.0 mmol) were dissolved in 0.5 mL of DMF. The reaction mixture was then stirred for 6 h at rt. Completion of reaction was confirmed by TLC, and column chromatography was performed to obtain pure compound **6** as semisolid (73%).^{1}H NMR (400 MHz, $CDCl_3$): δ 5.22 (s, 2H), 4.24 (t, J = 6.8 Hz, 2H), 4.07 (s, 3H), 3.94 (t, J = 7.2 Hz, 2H), 2.37−2.34 (m, 6H), 2.00−1.92 (m, 2H), 1.77−1.70 (m, 2H), 1.59−1.53 (m, 4H), 1.49−1.43 (m, 2H) 1.41−1.35 (m, 2H), 0.93 (t, J = 7.2 Hz, 3H). ^{13}C NMR (100 MHz, CDCl3): δ 160.8, 154.8, 153.7, 152.0, 110.9, 66.9, 56.7, 56.2, 54.5, 39.6, 31.2, 26.1, 25.7, 24.2, 19.3, 14.0. HRMS (ESI) m/z: (M + H) calcd for $C_{18}H_{31}N_6O_2$, 363.2508; found, 363.2512.

General Procedure C for Synthesis of 6-Amino-2-butoxy-9-(3-(piperidin-1-yl)propyl)-9*H*-purin-8-ol (7). Compound **6** (0.1 g, 0.03 mmol) was dissolved in 0.5 mL of 4 M HCl in dioxane at rt for 3 h. The reaction mixture was then neutralized with ammonia and concentrated in vacuum. Column chromatography was performed using 5% ammonia in methanol and $CHCl_3$ as a mobile phase to

https://dx.doi.org/10.1021/acs.jmedchem.0c00011
J. Med. Chem. 2020, 63, 4776−4789

obtain pure compound **7** as white solid (87%, mp > 250 °C). ^{1}H NMR (600 MHz, $CDCl_3$): δ 5.84 (s, 1H), 4.22 (t, J = 6.6 Hz, 2H), 3.87 (t, J = 6.6 Hz, 2H), 2.61−2.59 (m, 6H), 2.07−2.04 (m, 2H), 1.74−1.70 (m, 2H), 1.67−1.65 (m, 4H), 1.46−1.43 (m, 4H), 0.94 (t, J = 7.2 Hz, 3H). ^{13}C NMR (125 MHz, $CDCl_3$ + 1 drop CD_3OD): δ 160.7, 153.7, 149.7, 147.9, 99.0, 67.0, 55.8, 54.1, 38.0, 31.0, 25.0, 24.8, 23.5, 19.2, 13.8. HRMS (ESI) m/z: (M + H) calcd for $C_{17}H_{29}N_6O_2$, 349.2352; found, 349.2351. HPLC purity 97.9%.

Synthesis of 2-Butoxy-9-(3-(4-ethylpiperazin-1-yl)propyl)-8-methoxy-9*H*-purin-6-amine (8). Compound **6** (0.1 g, 0.3 mmol), potassium carbonate (0.1 g, 0.7 mmol), and ethylpiperazine (0.13 mL, 1.0 mmol) were dissolved in 0.5 mL of DMF. The reaction was then performed according to general procedure B to obtain pure compound **8** as semisolid (67%). ^{1}H NMR (400 MHz, $CDCl_3$): δ 5.31 (s, 2H), 4.22 (t, J = 6.4 Hz, 2H), 4.05 (s, 3H), 3.93 (t, J = 6.8 Hz, 2H), 2.48−2.32 (m, 12H), 1.93−1.88 (m, 2H), 1.74−1.67 (m, 2H), 1.49−1.41 (m, 2H), 1.03 (t, J = 7.2 Hz, 3H), 0.91 (t, J = 7.2 Hz, 3H). ^{13}C NMR (100 MHz, $CDCl_3$): δ 160.8, 154.8, 153.7, 151.9, 110.8, 66.9, 56.7, 55.5, 53.0, 52.7, 52.3, 39.6, 31.2, 26.2, 19.3, 13.9, 11.9. HRMS (ESI) m/z: (M + H) calcd for $C_{19}H_{34}N_7O_2$, 392.2774; found, 349.2773.

Synthesis of 6-Amino-2-butoxy-9-(3-(4-ethylpiperazin-1-yl)propyl)-9*H*-purin-8-ol (9). Compound **8** (0.1 g, 0.3 mmol) was dissolved in 0.5 mL of 4 M HCl in dioxane at rt for 3 h. The reaction was then performed according to general procedure C to obtain pure compound **9** as white solid (91%, mp > 250 °C). ^{1}H NMR (400 MHz, CD_3OD): δ 4.25 (t, J = 6.8 Hz, 2H), 3.85 (t, J = 6.8 Hz, 2H), 2.76−2.04 (m, 12H), 1.95−1.88 (m, 2H), 1.74−1.66 (m, 2H), 1.51−1.43 (m, 2H), 1.04 (t, J = 7.2 Hz, 3H), 0.94 (t, J = 7.2 Hz, 3H). ^{13}C NMR (100 MHz, CD_3OD): δ 160.8, 153.8, 149.9, 148.4, 98.5, 66.6, 55.5, 52.2, 52.0, 51.9, 38.2, 30.9, 24.8, 18.9, 12.8, 10.3. HRMS (ESI) m/z: (M + H) calcd for $C_{18}H_{32}N_7O_2$, 378.2617; found, 378.2617. HPLC purity 99.2%.

Synthesis of 8-Methoxy-9*H*-purin-6-amine (11). Compound **10** (0.2 g, 6.3 mmol) was refluxed with a 5 M solution of sodium methoxide in methanol (63 mmol, 10 mL) for 12 h. The reaction mixture was then concentrated in vacuum and diluted with 2 mL of water. The reaction mixture was neutralized, and the precipitation was filtered to obtain pure compound **11** as brown solid (72%, mp > 250 °C). ^{1}H NMR (400 MHz, DMSO-d_6): δ 8.06 (s, 1H), 7.38 (s, 2H), 6.81 (s, 1H), 3.98 (s, 3H). ^{13}C NMR (100 MHz, CD_3OD): δ 154.5, 151.4, 150.5, 148.5, 106.3, 57.2. HRMS (ESI) m/z: (M + H) calcd for $C_6H_8N_5O$, 166.0729; found, 166.0732.

Synthesis of 9-(3-Chloropropyl)-8-methoxy-9*H*-purin-6-amine (12). The reaction was performed according to general procedure A using compound **11** (0.2 g, 1.2 mmol), potassium carbonate (0.5 g, 3.6 mmol), and 1-bromo-3-chloropropane in 3 mL DMF to obtain compound **15** as white semisolid (78%). ^{1}H NMR (400 MHz, $CDCl_3$): δ 8.22 (s, 1H), 5.38 (s, 2H), 4.17−4.14 (m, 5H), 3.54−3.49 (m, 2H), 2.30−2.23 (m, 2H). ^{13}C NMR (100 MHz, CDCl3): δ 155.6, 152.9, 151.3, 150.2, 115.7, 57.2, 41.7, 39.0, 31.9. HRMS (ESI) m/z: (M + H) calcd for $C_6H_{13}N_5OCl$, 242.0809; found, 242.0809.

Synthesis of 9-(3-(4-Ethylpiperazin-1-yl)propyl)-8-methoxy-9*H*-purin-6-amine (13). Compound **12** (0.1 g, 0.4 mmol), potassium carbonate (0.1 g, 0.7 mmol), and ethylpiperazine (0.2 mL, 1.1 mmol) were dissolved in 0.5 mL of DMF. The reaction was then performed according to general procedure B to obtain pure compound **13** as semisolid (63%). ^{1}H NMR (300 MHz, $CDCl_3$): δ 8.21 (s, 1H), 5.49 (s, 2H), 4.12 (s, 3H), 4.04 (t, J = 6.9 Hz, 2H), 2.45−2.36 (m, 12H), 1.97−1.92 (m, 2H), 1.07 (t, J = 7.2 Hz, 3H). ^{13}C NMR (100 MHz, $CDCl_3$): δ 155.8, 152.8, 151.1, 150.3, 115.7, 56.9, 55.5, 52.9, 52.8, 52.3, 39.9, 26.2, 11.8. HRMS (ESI) m/z: (M + H) calcd for $C_{15}H_{26}N_7O$, 320.2199; found, 320.2195.

Synthesis of 6-Amino-9-(3-(4-ethylpiperazin-1-yl)propyl)-9*H*-purin-8-ol (14). Compound **13** (0.1 g, 0.3 mmol) was dissolved in 0.5 mL of 4 M HCl in dioxane at rt for 3 h. The reaction was then performed according to general procedure C to obtain pure compound **14** as white semisolid (86%). ^{1}H NMR (300 MHz, CD_3OD): δ 8.09 (s, 1H), 3.95 (t, J = 6.6 Hz, 2H), 2.49−2.40 (m, 12H), 2.02−1.93 (m, 2H), 1.04 (t, J = 7.2 Hz, 3H). ^{13}C NMR (100 MHz, CD_3OD): δ 153.5, 150.9, 147.9, 147.1, 100.0, 55.5, 52.2, 51.9, 51.8, 38.3, 24.7, 10.3. HRMS (ESI) m/z: (M + H) calcd for $C_{14}H_{24}N_7O$, 306.2042; found, 306.2038. HPLC purity 97.7%.

6-Chloro-9-(3-(4-ethylpiperazin-1-yl)propyl)-9*H*-purine (16). Compound **15** (0.1 g, 0.7 mmol) and 1-(3-chloropropyl)-4-ethylpiperazine (0.3 g, 1.2 mmol) were taken in dry 0.5 mL of DMF and potassium carbonate (0.2 g, 1.2 mmol) was added to it. The reaction mixture was heated at 60 °C for 12 h. Water was added to the reaction mixture. The aqueous solution was extracted with chloroform and the organic layer was dried over Na_2SO_4 and evaporated under vacuum. The residue was purified by silica gel column chromatography eluting with 4% methanol in chloroform to provide compound **16** as semisolid (84%). ^{1}H NMR (300 MHz, $CDCl_3$): δ 8.74 (s, 1H), 8.17 (s, 1H), 4.38 (t, J = 6.6 Hz, 2H), 2.51−2.37 (m, 8H), 2.30 (t, J = 6.6 Hz, 2H), 2.10−2.07 (m, 2H), 1.75−1.69 (m, 2H), 1.08 (t, J = 7.2 Hz, 3H). ^{13}C NMR (75 MHz, $CDCl_3$): δ 151.9, 151.8, 150.9, 145.9, 131.7, 54.2, 52.4, 52.3, 52.2, 42.4, 29.7, 26.0, 11.5. HRMS (ESI) m/z: (M + H) calcd for $C_{14}H_{22}ClN_6$, 309.1594; found, 309.1588.

9-(3-(4-Ethylpiperazin-1-yl)propyl)-9*H*-purin-6-amine (17). Compound **16** (0.1 g, 0.3 mmol) and 2 mL of ammonia in ethanol (7 equiv) were taken in a pressure tube. The reaction mixture was heated at 60 °C for 12 h. Ethanol was evaporated, and residue was purified by column chromatography to obtain compound **17** as semisolid (67%). ^{1}H NMR (400 MHz, $CDCl_3$ + CD_3OD): δ 8.10 (s, 1H), 7.79 (s, 1H), 4.14 (t, J = 6.8 Hz, 2H), 3.01−2.81 (m, 6H), 2.70−2.53 (m, 4H), 2.36 (t, J = 6.8 Hz, 2H), 1.97−190 (m, 2H), 1.20 (t, J = 7.2 Hz, 3H). ^{13}C NMR (100 MHz, $CDCl_3$ + CD_3OD): δ 156.6, 153.5, 145.0, 123.0, 100.0, 57.0, 56.0, 55.2, 53.8, 53.7, 45.8, 30.3, 13.2, 4.8. HRMS (ESI) m/z: (M + H) calcd for $C_{14}H_{24}N_7$, 290.2093; found, 290.2084. HPLC purity 99.6%.

9-(3-(4-Ethylpiperazin-1-yl)propyl)-9*H*-purin-6-amine (18). Compound **16** (0.1 g, 0.3 mmol) was dissolved in 10 mL of tetrahydrofuran (THF), and solution was degassed using argon. 10% palladium on carbon (10 mol %) was added to the reaction mixture and then the reaction mixture was stirred at rt under a hydrogen atmosphere for 1 h. Completion of the reaction was confirmed by monitoring TLC, and the catalyst was separated using Celite filtration. The filtrate was evaporated, and the residue was purified by column chromatography to obtain compound **18** as semisolid (91%). ^{1}H NMR (400 MHz, $CDCl_3$): δ 9.13 (s, 1H), 8.98 (s, 1H), 8.13 (s, 1H), 4.38 (t, J = 6.6 Hz, 2H), 2.58−2.38 (m, 10H), 2.32 (t, J = 6.6 Hz, 2H), 2.13−2.05 (m, 2H), 1.08 (t, J = 7.2 Hz, 3H). ^{13}C NMR (150 MHz, $CDCl_3$): δ 152.5, 151.4, 148.5, 145.9, 134.1, 54.4, 52.6, 52.3, 41.7, 26.2, 11.7. HRMS (ESI) m/z: (M + H) calcd for $C_{14}H_{23}N_6$, 275.1984; found, 275.1973. HPLC purity 96.4%.

9-(3-(4-Ethylpiperazin-1-yl)propyl)-*N*,*N*-dimethyl-9*H*-purin-6-amine (19). Compound **16** (0.1 g, 0.3 mmol) and 2 mL of dimethylamine in THF (2 M) were added to 3 mL of acetonitrile in presence of base potassium carbonate (0.06 g, 0.62 mmol) The reaction mixture was refluxed for 12 h and then solvent was evaporated and column chromatography was performed to obtain pure compound **19** as semisolid (89%). ^{1}H NMR (400 MHz, $CDCl_3$): δ 8.31 (s, 1H), 7.71 (s, 1H), 4.22 (t, J = 6.8 Hz, 2H), 3.50 (s, 6H), 2.44−2.37 (m, 10H), 2.28 (t, J = 6.8 Hz, 2H), 2.04−1.99 (m, 2H), 1.07 (t, J = 7.2 Hz, 3H). ^{13}C NMR (100 MHz, $CDCl_3$): δ 155.0, 152.4, 150.6, 138.8, 120.3, 54.5, 52.9, 52.8, 52.4, 41.6, 26.6, 11.9. HRMS (ESI) m/z: (M + H) calcd for $C_{16}H_{26}N_7$, 318.2406; found, 318.2404. HPLC purity 98.6%.

General Procedure C 9-(3-(4-Ethylpiperazin-1-yl)propyl)-6-(piperidin-1-yl)-9*H*-purine (20). Compound **16** (0.1 g, 0.2 mmol) was dissolved in acetonitrile (1 mL), and potassium carbonate (0.04 g, 0.28 mmol) and piperidine (0.02 g, 1.2 mmol) were added. The reaction was refluxed under the N_2 atmospheric condition for 12 h. The organic layer was extracted with a $CHCl_3$ system, and column chromatography was done by using CH_3OH and $CHCl_3$ systems to give compound **20** (73%) as a semisolid. ^{1}H NMR (400 MHz, $CDCl_3$): δ 8.29 (s, 1H), 7.72 (s, 1H), 4.24−4.20 (m, 6H), 2.51−2.41 (m, 8H), 2.31 (t, J = 6.8 Hz, 2H), 2.05−1.98 (m, 4H), 1.70−1.65 (m, 6H), 1.08 (t, J = 7.2 Hz, 3H). ^{13}C NMR (100 MHz, $CDCl_3$): δ 154.0,

https://dx.doi.org/10.1021/acs.jmedchem.0c00011
J. Med. Chem. 2020, 63, 4776−4789

152.4, 150.8, 138.6, 119.9, 54.5, 52.8, 52.7, 52.4, 41.6, 26.6, 26.2, 24.9, 11.8. HRMS (ESI) *m/z*: (M + H) calcd for $C_{19}H_{32}N_7$, 358.2719; found, 358.2721. HPLC purity 95.6%.

4-(9-(3-(4-Ethylpiperazin-1-yl)propyl)-9*H*-purin-6-yl)-morpholine (21). Compound **16** (0.1 g, 0.2 mmol) was dissolved in acetonitrile (1 mL), and potassium carbonate (0.04 g, 0.28 mmol) and morpholine (0.03 g, 1.2 mmol) were added. The reaction then proceeds according to general procedure C to get compound **21** (82%) as a semisolid. ^{1}H NMR (600 MHz, $CDCl_3$): δ 8.35 (s, 1H), 7.76 (s, 1H), 4.33−4.30 (m, 4H), 4.26 (t, J = 6.6 Hz, 2H), 3.83 (t, J = 4.8 Hz, 4H), 2.49−2.40 (m, 8H), 2.31 (t, J = 6.6 Hz, 2H), 2.06−2.02 (m, 2H), 1.97−1.91 (m, 2H), 1.08 (t, J = 7.2 Hz, 3H). ^{13}C NMR (150 MHz, $CDCl_3$): δ 156.4, 154.7, 153.4, 141.6, 122.5, 69.5, 56.8, 55.3, 55.2, 54.7, 43.9, 28.8, 14.3. HRMS (ESI) *m/z*: (M + H) calcd for $C_{18}H_{30}N_7O$, 360.2512; found, 360.2523. HPLC purity 95.1%.

9-(3-(4-Ethylpiperazin-1-yl)propyl)-6-(piperazin-1-yl)-9*H*-purine (22). Compound **16** (0.1 g, 0.2 mmol) was dissolved in acetonitrile (1 mL), and potassium carbonate (0.04 g, 0.28 mmol) and piperazine (0.1 g, 1.2 mmol) were added. The reaction then proceeds according to general procedure C to get compound **22** (86%) as a semisolid. ^{1}H NMR (600 MHz, $CDCl_3$): δ 8.30 (s, 1H), 7.72 (s, 1H), 4.27−4.21 (m, 6H), 3.00−2.95 (m, 4H), 2.49−2.33 (m, 10H), 2.27 (t, J = 6.6 Hz, 2H), 2.04−1.98 (m, 2H), 1.05 (t, J = 7.2 Hz, 3H). ^{13}C NMR (150 MHz, $CDCl_3$): δ 156.4, 154.7, 153.3, 141.3, 122.4, 56.8, 55.4, 55.2, 54.7, 48.7, 43.7, 28.8, 14.4. HRMS (ESI) *m/z*: (M + H) calcd for $C_{18}H_{31}N_8$, 359.2672; found, 35.92675. HPLC purity 99.4%.

6-(4-Ethylpiperazin-1-yl)-9-(3-(4-ethylpiperazin-1-yl)-propyl)-9*H*-purine (23). Compound **16** (0.5 g, 0.7 mmol) was dissolved in acetonitrile (8 mL), and potassium carbonate (0.2 g, 1.5 mmol) and ethylpiperazine (0.13 mL, 1.2 mmol) were added. The reaction then proceeds according to general procedure C to get compound **23** (95%) as a semisolid. ^{1}H NMR (300 MHz, $CDCl_3$): δ 8.34 (s, 1H), 7.76 (s, 1H), 4.43−4.29 (m, 4H), 4.25 (t, J = 6.6 Hz, 2H), 2.60−2.57 (m, 4H), 2.51−2.39 (m, 12H), 2.31 (t, J = 6.6 Hz, 2H), 2.08−2.01 (m, 2H), 1.16−1.06 (m, 6H). ^{13}C NMR (150 MHz, $CDCl_3$): δ 153.9, 152.3, 150.9, 138.9, 120.0, 54.4, 53.0, 52.8, 52.7, 52.5, 52.3, 41.5, 26.5, 12.0. HRMS (ESI) *m/z*: (M + H) calcd for $C_{20}H_{35}N_8$, 387.2985; found, 387.2979. HPLC purity 99.2%.

6-(4-Cyclopentylpiperazin-1-yl)-9-(3-(4-ethylpiperazin-1-yl)propyl)-9*H*-purine (24). Compound **16** (0.1 g, 0.4 mmol) was dissolved in acetonitrile (1 mL), and potassium carbonate (0.05 g, 0.4 mmol) and piperazine (0.03 g, 0.34 mmol) were added. The reaction then proceeds according to general procedure C to get compound **24** (86%) as a semisolid. ^{1}H NMR (300 MHz, $CDCl_3$): δ 8.33 (s, 1H), 7.74 (s, 1H), 4.46−4.30 (m, 4H), 4.25 (t, J = 6.6 Hz, 2H), 2.71−2.55 (m, 13H), 2.36 (t, J = 6.9 Hz, 2H), 2.09−2.00 (m, 2H), 1.91−1.87 (m, 4H), 1.78−1.68 (m, 2H), 1.62−1.49 (m, 4H), 1.19 (t, J = 7.2 Hz, 3H). ^{13}C NMR (150 MHz, $CDCl_3$): δ 153.7, 152.3, 150.9, 138.8, 119.9, 67.6, 54.2, 52.3, 52.2, 51.6, 41.5, 30.1,26.4, 23.9, 24.0, 10.9. HRMS (ESI) *m/z*: (M + H) calcd for $C_{23}H_{39}N_8$, 427.3298; found, 427.3297. HPLC purity 97.3%.

9-(3-Chloropropyl)-6-(4-ethylpiperazin-1-yl)-9*H*-purine (26). Compound **25** (1.6 g, 6.7 mmol) and potassium carbonate (1.9 g, 14 mmol) were dissolved in 1 mL of DMF, and the reaction mixture was heated at 50 °C for 2 h. 1-Bromo-3-chloropropane was added to the reaction mixture at rt and stirred for 12 h. The solvent was then removed and the reaction was partitioned between $CHCl_3$ and water. The organic layer was then dried, and column chromatography was performed to get pure compound **5** as semisolid (71%). ^{1}H NMR (300 MHz, $CDCl_3$): δ 8.17 (s, 1H), 7.63 (s, 1H), 4.25−4.12 (m, 6H), 3.35 (t, J = 6.0 Hz, 2H), 3.43 (t, J = 5.1 Hz, 4H), 2.35−2.28 (m, 2H), 2.25−2.16 (m, 2H), 0.98 (t, J = 7.2 Hz, 3H). ^{13}C NMR (100 MHz, $CDCl_3$): δ 153.8, 152.4, 150.7, 138.5, 120.1, 52.8, 52.4, 41.4, 40.8, 31.8, 11.9. HRMS (ESI) *m/z*: (M + H) calcd for $C_{14}H_{22}N_6Cl$, 309.1594; found, 309.1599.

6-(4-Ethylpiperazin-1-yl)-9-(3-(piperazin-1-yl)propyl)-9*H*-purine (27). Compound **26** (0.1 g, 0.3 mmol), potassium carbonate (0.1 g, 0.7 mmol), and piperidine (0.11 mL, 1.0 mmol) were dissolved in 0.5 mL of DMF. The reaction was then performed according to general procedure B to obtain pure compound **8** as semisolid (78%). ^{1}H NMR (400 MHz, $CDCl_3$): δ 8.29 (s, 1H), 8.10 (s, 1H), 4.56−4.41 (m, 4H), 4.31 (t, J = 6.8 Hz, 2H), 3.12 (t, J = 5.2 Hz, 8H), 2.99−2.95 (m, 2H), 2.60−2.58 (m, 4H), 2.41 (t, J = 6.8 Hz, 2H), 2.08−2.01 (m, 2H), 1.19 (t, J = 7.2 Hz, 3H). ^{13}C NMR (150 MHz, $CDCl_3$): δ 155.8, 154.0, 153.3, 143.2, 122.2, 56.7, 54.4, 53.9, 51.7, 45.9, 43.9, 28.4, 11.4. HRMS (ESI) *m/z*: (M + H) calcd for $C_{18}H_{31}N_8$, 359.2672; found, 359.2675. HPLC purity 95.4%.

4-(3-(6-(4-Ethylpiperazin-1-yl)-9*H*-purin-9-yl)propyl)-morpholine (28). Compound **26** (0.1 g, 0.3 mmol), potassium carbonate (0.1 g, 0.7 mmol), and morpholine (0.09 mL, 1.0 mmol) were dissolved in 0.5 mL of DMF. The reaction was then performed according to general procedure B to obtain pure compound **8** as semisolid (85%). ^{1}H NMR (300 MHz, $CDCl_3$): δ 8.31 (s, 1H), 7.72 (s, 1H), 4.34−4.31 (m, 4H), 4.24 (t, J = 6.8 Hz, 2H), 3.68−3.66 (m, 4H), 2.59−2.57 (m, 4H), 2.50−2.45 (m, 2H), 2.38−2.36 (m, 4H), 2.27 (t, J = 6.8 Hz, 2H), 2.05−1.98 (m, 2H), 1.12 (t, J = 7.2 Hz, 3H). ^{13}C NMR (150 MHz, $CDCl_3$): δ 153.8, 152.3, 150.9, 138.8, 120.0, 66.9, 54.9, 53.5, 52.8, 52.4, 41.5, 29.6, 26.1, 11.8. HRMS (ESI) *m/z*: (M + H) calcd for $C_{18}H_{30}N_7O$, 360.2512; found, 360.2523. HPLC purity 96.0%.

6-(4-Ethylpiperazin-1-yl)-9-(3-(piperidin-1-yl)propyl)-9*H*-purine (29). Compound **26** (0.1 g, 0.3 mmol), potassium carbonate (0.1 g, 0.7 mmol), and piperidine (0.11 mL, 1.0 mmol) were dissolved in 0.5 mL of DMF. The reaction was then performed according to general procedure B to obtain pure compound **8** as semisolid (93%). ^{1}H NMR (600 MHz, $CDCl_3$): δ 8.33 (s, 1H), 7.75 (s, 1H), 4.41−4.39 (m, 4H), 4.24 (t, J = 6.6 Hz, 2H), 2.59−2.57 (m, 4H), 2.49−2.45 (m, 2H), 2.42−2.35 (m, 4H), 2.31 (t, J = 6.6 Hz, 2H), 2.07−2.03 (m, 2H), 1.60−1.55 (m, 4H), 1.47−1.41 (m, 2H), 1.13 (t, J = 7.2 Hz, 3H). ^{13}C NMR (150 MHz, $CDCl_3$): δ 153.8, 152.2, 150.8, 138.9, 119.9, 55.0, 54.3, 52.9, 52.4, 41.5, 26.4, 25.6, 24.1, 11.8. HRMS (ESI) *m/z*: (M + H) calcd for $C_{19}H_{32}N_7$, 358.2719; found, 358.2713. HPLC purity 96.8%.

6-(4-Ethylpiperazin-1-yl)-9-(3-(pyrrolidin-1-yl)propyl)-9*H*-purine (30). Compound **26** (0.1 g, 0.3 mmol), potassium carbonate (0.1 g, 0.7 mmol), and pyrrolidine (0.08 mL, 1.0 mmol) were dissolved in 0.5 mL of DMF. The reaction was then performed according to general procedure B to obtain pure compound **8** as semisolid (93%). ^{1}H NMR (400 MHz, $CDCl_3$): δ 8.30 (s, 1H), 7.74 (s, 1H), 4.38−4.28 (m, 4H), 4.25 (t, J = 6.8 Hz, 2H), 2.55 (t, J = 5.2 Hz, 4H), 2.48−2.41 (m, 8H), 2.08−2.00 (m, 2H), 1.77−1.72 (m, 4H), 1.10 (t, J = 7.2 Hz, 3H). ^{13}C NMR (100 MHz, $CDCl_3$): δ 153.9, 152.4, 150.9, 138.9, 120.0, 54.1, 53.0, 52.6, 52.5, 41.7, 28.7, 23.5, 12.0. HRMS (ESI) *m/z*: (M + H) calcd for $C_{18}H_{30}N_7$, 344.2563; found, 344.2569. HPLC purity 95.8%.

6-(4-Ethylpiperazin-1-yl)-9-propyl-9*H*-purine (31). Compound **25** (1.0 g, 4.3 mmol) and potassium carbonate (1.2 g, 8.6 mmol) were dissolved in 1 mL of DMF, and the reaction mixture was heated at 50 °C for 2 h. 3-Bromopropane (0.7 mL, 6.5 mmol) was added to the reaction mixture at rt and stirred for 12 h. The solvent was then removed, and reaction was partitioned between $CHCl_3$ and water. Organic layer was then dried, and column chromatography was performed to get pure compound **5** as semisolid (78%). ^{1}H NMR (400 MHz, $CDCl_3$): δ 8.35 (s, 1H), 7.73 (s, 1H), 4.44−4.26 (m, 4H), 4.14 (t, J = 7.2 Hz, 2H), 2.61−2.57 (m, 4H), 2.51−2.44 (m, 2H), 1.94−1.87 (m, 2H), 1.13 (t, J = 7.2 Hz, 3H), 0.96 (t, J = 7.2 Hz, 3H). ^{13}C NMR (100 MHz, $CDCl_3$): δ 153.9, 152.3, 150.9, 138.4, 119.9, 52.9, 52.5, 45.4, 23.4, 11.9, 11.2. HRMS (ESI) *m/z*: (M + H) calcd for $C_{14}H_{23}N_6$, 275.1984; found, 275.1977. HPLC purity 96.9%.

■ ASSOCIATED CONTENT

Supporting Information

The Supporting Information is available free of charge at https://pubs.acs.org/doi/10.1021/acs.jmedchem.0c00011.

TLR7 antagonistic assay, TLR7 agonistic assay, TLR8 antagonistic assay, cytotoxicity assay, X-ray crystallographic structure of HCl salt of compound **16**, LC−MS/

https://dx.doi.org/10.1021/acs.jmedchem.0c00011
J. Med. Chem. 2020, 63, 4776−4789

MS spectrum analysis of compound **23**, aqueous solubility assay table, Caco-2 permeability assay table, plasma stability assay table, microsomal stability assay table, molecular docking, HPLC data, and ^{1}H NMR and ^{13}C NMR spectra of compounds **1**−**31** (PDF)

Molecular formula strings (CSV)

Human TLR7 homology model (PDB)

AUTHOR INFORMATION

Corresponding Authors

Dipyaman Ganguly − *IICB-Translational Research Unit of Excellence, CSIR-Indian Institute of Chemical Biology, Kolkata 700032, India; Academy of Scientific and Innovative Research (AcSIR), Ghaziabad 201002, India*; Email: dipyaman@iicb.res.in

Arindam Talukdar − *Department of Organic and Medicinal Chemistry, CSIR-Indian Institute of Chemical Biology, Kolkata 700032, West Bengal, India; Academy of Scientific and Innovative Research (AcSIR), Ghaziabad 201002, India*; orcid.org/0000-0002-7831-1795; Email: atalukdar@iicb.res.in

Authors

Ayan Mukherjee − *Department of Organic and Medicinal Chemistry, CSIR-Indian Institute of Chemical Biology, Kolkata 700032, West Bengal, India; Academy of Scientific and Innovative Research (AcSIR), Ghaziabad 201002, India*

Deblina Raychaudhuri − *IICB-Translational Research Unit of Excellence, CSIR-Indian Institute of Chemical Biology, Kolkata 700032, India*

Bishnu Prasad Sinha − *IICB-Translational Research Unit of Excellence, CSIR-Indian Institute of Chemical Biology, Kolkata 700032, India*

Biswajit Kundu − *Department of Organic and Medicinal Chemistry, CSIR-Indian Institute of Chemical Biology, Kolkata 700032, West Bengal, India*

Mousumi Mitra − *IICB-Translational Research Unit of Excellence, CSIR-Indian Institute of Chemical Biology, Kolkata 700032, India*

Barnali Paul − *Department of Organic and Medicinal Chemistry, CSIR-Indian Institute of Chemical Biology, Kolkata 700032, West Bengal, India; Academy of Scientific and Innovative Research (AcSIR), Ghaziabad 201002, India*

Purbita Bandopadhyay − *IICB-Translational Research Unit of Excellence, CSIR-Indian Institute of Chemical Biology, Kolkata 700032, India; Academy of Scientific and Innovative Research (AcSIR), Ghaziabad 201002, India*

Complete contact information is available at: https://pubs.acs.org/10.1021/acs.jmedchem.0c00011

Author Contributions

‖A.M., D.R., and B.P.S. contributed equally.

Notes

The authors declare no competing financial interest.

ACKNOWLEDGMENTS

The project was supported by grant no. EMR/2016/003021 from Science and Engineering Research Board (SERB), Department of Science & Technology (DST), Govt. of India, to D.G. and A.T. Acknowledging University Grant Commission (UGC), Govt. of India by A.M., B.P. and B.K. for fellowship. D.R. would like to acknowledge Council of Scientific and Industrial Research (CSIR) for her SPM senior research fellowship. P.B. would like to acknowledge Council of Scientific and Industrial Research (CSIR). B.P.S. is supported by the SyMeC Biocluster project from Department of Biotechnology (DBT), Govt. of India. Authors would like to acknowledge Central Instrument Facility of CSIR-IICB and Santu Paul for the LTQ Orbitrap XL mass spectrometer.

ABBREVIATIONS

pDC, plasmacytoid dendritic cell; SLE, systemic lupus erythematosus; hPBMC, human peripheral blood mononuclear cell; LC−MS, liquid chromatography−mass spectrometry; ISG15, interferon-stimulated gene 15; DMEM, Dulbecco's modified Eagle medium; HBSS, Hank's balanced salt solution; SEAP, secreted alkaline phosphatase; IFN, interferon

REFERENCES

(1) Pandey, S.; Kawai, T.; Akira, S. Microbial sensing by toll-like receptors and intracellular nucleic acid sensors. *Cold Spring Harbor Perspect. Biol.* **2015**, *7*, a016246.

(2) Takeda, K.; Kaisho, T.; Akira, S. Toll-like receptors. *Annu. Rev. Immunol.* **2003**, *21*, 335−376.

(3) Akira, S.; Uematsu, S.; Takeuchi, O. Pathogen recognition and innate immunity. *Cell* **2006**, *124*, 783−801.

(4) Gilliet, M.; Cao, W.; Liu, Y.-J. Plasmacytoid dendritic cells: sensing nucleic acids in viral infection and autoimmune diseases. *Nat. Rev. Immunol.* **2008**, *8*, 594−606.

(5) Akira, S.; Takeda, K. Toll-like receptor signalling. *Nat. Rev. Immunol.* **2004**, *4*, 499−511.

(6) Gay, N. J.; Symmons, M. F.; Gangloff, M.; Bryant, C. E. Assembly and localization of toll-like receptor signalling complexes. *Nat. Rev. Immunol.* **2014**, *14*, 546−558.

(7) Lande, R.; Gregorio, J.; Facchinetti, V.; Chatterjee, B.; Wang, Y.-H.; Homey, B.; Cao, W.; Wang, Y.-H.; Su, B.; Nestle, F. O.; Zal, T.; Mellman, I.; Schröder, J.-M.; Liu, Y.-J.; Gilliet, M. Plasmacytoid dendritic cells sense self-DNA coupled with antimicrobial peptide. *Nature* **2007**, *449*, 564−569.

(8) Ganguly, D.; Chamilos, G.; Lande, R.; Gregorio, J.; Meller, S.; Facchinetti, V.; Homey, B.; Barrat, F. J.; Zal, T.; Gilliet, M. Self-RNA-antimicrobial peptide complexes activate human dendritic cells through TLR7 and TLR8. *J. Exp. Med.* **2009**, *206*, 1983−1994.

(9) Lande, R.; Ganguly, D.; Facchinetti, V.; Frasca, L.; Conrad, C.; Gregorio, J.; Meller, S.; Chamilos, G.; Sebasigari, R.; Riccieri, V.; Bassett, R.; Amuro, H.; Fukuhara, S.; Ito, T.; Liu, Y.-J.; Gilliet, M. Neutrophils activate plasmacytoid dendritic cells by releasing self-DNA-peptide complexes in systemic lupus erythematosus. *Sci. Transl. Med.* **2011**, *3*, 73ra19.

(10) Ganguly, D.; Haak, S.; Sisirak, V.; Reizis, B. The role of dendritic cells in autoimmunity. *Nat. Rev. Immunol.* **2013**, *13*, 566−577.

(11) Ganguly, D. Do type I interferons link systemic autoimmunities and metabolic syndrome in a pathogenetic continuum? *Trends Immunol.* **2018**, *39*, 28−43.

(12) Czarniecki, M. Small molecule modulators of toll-like receptors. *J. Med. Chem.* **2008**, *51*, 6621−6626.

(13) Lipford, B.; Forsbach, D.; Zepp, C. M. Small Molecule Toll-like Receptor (TLR) Antagonists. U.S. Patent 20,070,232,622 A1, 2007.

(14) Zhang, L.; Dewan, V.; Yin, H. Discovery of small molecules as multi-toll-like receptor agonists with proinflammatory and anticancer activities. *J. Med. Chem.* **2017**, *60*, 5029−5044.

(15) Van der Fits, L.; Mourits, S.; Voerman, J. S. A.; Kant, M.; Boon, L.; Laman, J. D.; Cornelissen, F.; Mus, A.-M.; Florencia, E.; Prens, E. P.; Lubberts, E. Imiquimod-induced psoriasis-like skin inflammation in mice is mediated via the IL-23/IL-17 axis. *J. Immunol.* **2009**, *182*, 5836−5845.

(16) Balak, D. M. W.; van Doorn, M. B. A.; Arbeit, R. D.; Rijneveld, R.; Klaassen, E.; Sullivan, T.; Brevard, J.; Thio, H. B.; Prens, E. P.;

Burggraaf, J.; Rissmann, R. IMO-8400, a Toll-like receptor 7, 8, and 9 antagonist, demonstrates clinical activity in a phase 2a, randomized, placebo-controlled trial in patients with moderate-to-severe plaque psoriasis. *Clin. Immunol.* **2017**, *174*, 63−72.
(17) Dosa, P. I.; Amin, E. A. Tactical approaches to interconverting GPCR agonists and antagonists. *J. Med. Chem.* **2016**, *59*, 810−840.
(18) Shukla, N. M.; Kimbrell, M. R.; Malladi, S. S.; David, S. A. Regioisomerism-dependent TLR7 agonism and antagonism in an imidazoquinoline. *Bioorg. Med. Chem. Lett.* **2009**, *19*, 2211−2214.
(19) Zhang, S.; Hu, Z.; Tanji, H.; Jiang, S.; Das, N.; Li, J.; Sakaniwa, K.; Jin, J.; Bian, Y.; Ohto, U.; Shimizu, T.; Yin, H. Small-molecule inhibition of TLR8 through stabilization of its resting state. *Nat. Chem. Biol.* **2018**, *14*, 58−64.
(20) Black, J. A life in new drug research. *Br. J. Pharmacol.* **2010**, *160*, S15−S25.
(21) Ganellin, R. Medicinal chemistry and dynamic structure−activity analysis in the discovery of drugs acting at histamine H_2-receptors. *J. Med. Chem.* **1981**, *24*, 913−920.
(22) Martin, W. History and development of mixed opioid agonists, partial agonists and antagonists. *Br. J. Clin. Pharmacol.* **1979**, *7*, 273S−279S.
(23) Biggadike, K.; Ahmed, M.; Ball, D. I.; Coe, D. M.; Dalmas Wilk, D. A.; Edwards, C. D.; Gibbon, B. H.; Hardy, C. J.; Hermitage, S. A.; Hessey, J. O.; Hillegas, A. E.; Hughes, S. C.; Lazarides, L.; Lewell, X. Q.; Lucas, A.; Mallett, D. N.; Price, M. A.; Priest, F. M.; Quint, D. J.; Shah, P.; Sitaram, A.; Smith, S. A.; Stocker, R.; Trivedi, N. A.; Tsitoura, D. C.; Weller, V. Discovery of 6-amino-2-{[(1*S*)-1-methylbutyl]oxy}-9-[5-(1-piperidinyl)pentyl]-7,9-dihydro-8*H*-purin-8-one (GSK2245035), a highly potent and selective intranasal toll-like receptor 7 agonist for the treatment of asthma. *J. Med. Chem.* **2016**, *59*, 1711−1726.
(24) Jones, P.; Pryde, D. C.; Tran, T.-D.; Adam, F. M.; Bish, G.; Calo, F.; Ciaramella, G.; Dixon, R.; Duckworth, J.; Fox, D. N. A.; Hay, D. A.; Hitchin, J.; Horscroft, N.; Howard, M.; Laxton, C.; Parkinson, T.; Parsons, G.; Proctor, K.; Smith, M. C.; Smith, N.; Thomas, A. Discovery of a highly potent series of TLR7 agonists. *Bioorg. Med. Chem. Lett.* **2011**, *21*, 5939−5943.
(25) Hirota, K.; Kazaoka, K.; Niimoto, I.; Kumihara, H.; Sajiki, H.; Isobe, Y.; Takaku, H.; Tobe, M.; Ogita, H.; Ogino, T.; Ichii, S.; Kurimoto, A.; Kawakami, H. Discovery of 8-hydroxyadenines as a novel type of interferon inducer. *J. Med. Chem.* **2002**, *45*, 5419−5422.
(26) Tran, T.-D.; Pryde, D. C.; Jones, P.; Adam, F. M.; Benson, N.; Bish, G.; Calo, F.; Ciaramella, G.; Dixon, R.; Duckworth, J.; Fox, D. N. A.; Hay, D. A.; Hitchin, J.; Horscroft, N.; Howard, M.; Gardner, I.; Jones, H. M.; Laxton, C.; Parkinson, T.; Parsons, G.; Proctor, K.; Smith, M. C.; Smith, N.; Thomas, A. Design and optimisation of orally active TLR7 agonists for the treatment of hepatitis C virus infection. *Bioorg. Med. Chem. Lett.* **2011**, *21*, 2389−2393.
(27) Zhang, Z.; Ohto, U.; Shibata, T.; Krayukhina, E.; Taoka, M.; Yamauchi, Y.; Tanji, H.; Isobe, T.; Uchiyama, S.; Miyake, K.; Shimizu, T. Structural analysis reveals that toll-like receptor 7 is a dual receptor for guanosine and single-stranded RNA. *Immunity* **2016**, *45*, 737−748.
(28) Zhang, Z.; Ohto, U.; Shibata, T.; Taoka, M.; Yamauchi, Y.; Sato, R.; Shukla, N. M.; David, S. A.; Isobe, T.; Miyake, K.; Shimizu, T. Structural analyses of toll-like receptor 7 reveal detailed RNA sequence specificity and recognition mechanism of agonistic ligands. *Cell Rep.* **2018**, *25*, 3371−3381.
(29) Isobe, Y.; Tobe, M.; Ogita, H.; Kurimoto, A.; Ogino, T.; Kawakami, H.; Takaku, H.; Sajiki, H.; Hirota, K.; Hayashi, H. Synthesis and structure−activity relationships of 2-substituted-8-hydroxyadenine derivatives as orally available interferon inducers without emetic side effects. *Bioorg. Med. Chem.* **2003**, *11*, 3641−3647.
(30) Bazin, H. G.; Li, Y.; Khalaf, J. K.; Mwakwari, S.; Livesay, M. T.; Evans, J. T.; Johnson, D. A. Structural requirements for TLR7-selective signaling by 9-(4-Piperidinylalkyl)-8-oxoadenine derivatives. *Bioorg. Med. Chem. Lett.* **2015**, *25*, 1318−1323.
(31) Smith, A. J.; Li, Y.; Bazin, H. G.; St-Jean, J. R.; Larocque, D.; Evans, J. T.; Baldridge, J. R. Evaluation of novel synthetic TLR7/8 agonists as vaccine adjuvants. *Vaccine* **2016**, *34*, 4304−4312.
(32) Isobe, Y.; Kurimoto, A.; Tobe, M.; Hashimoto, K.; Nakamura, T.; Norimura, K.; Ogita, H.; Takaku, H. Synthesis and biological evaluation of novel 9-substituted-8-hydroxyadenine derivatives as potent interferon inducers. *J. Med. Chem.* **2006**, *49*, 2088−2095.
(33) Roethle, P. A.; McFadden, R. M.; Yang, H.; Hrvatin, P.; Hui, H.; Graupe, M.; Gallagher, B.; Chao, J.; Hesselgesser, J.; Duatschek, P.; Zheng, J.; Lu, B.; Tumas, D. B.; Perry, J.; Halcomb, R. L. Identification and optimization of pteridinone toll-like receptor 7 (TLR7) agonists for the oral treatment of viral hepatitis. *J. Med. Chem.* **2013**, *56*, 7324−7333.
(34) Lamphier, M.; Zheng, W.; Latz, E.; Spyvee, M.; Hansen, H.; Rose, J.; Genest, M.; Yang, H.; Shaffer, C.; Zhao, Y.; Shen, Y.; Liu, C.; Liu, D.; Mempel, T. R.; Rowbottom, C.; Chow, J.; Twine, N. C.; Yu, M.; Gusovsky, F.; Ishizaka, S. T. Novel small molecule inhibitors of TLR7 and TLR9: mechanism of action and efficacy in vivo. *Mol. Pharmacol.* **2014**, *85*, 429−440.
(35) Paul, B.; Rahaman, O.; Roy, S.; Pal, S.; Satish, S.; Mukherjee, A.; Ghosh, A. R.; Raychaudhuri, D.; Bhattacharya, R.; Goon, S.; Ganguly, D.; Talukdar, A. Activity-guided development of potent and selective toll-like receptor 9 antagonists. *Eur. J. Med. Chem.* **2018**, *159*, 187−205.
(36) Gerster, J. F.; Lindstrom, K. J.; Miller, R. L.; Tomai, M. A.; Birmachu, W.; Bomersine, S. N.; Gibson, S. J.; Imbertson, L. M.; Jacobson, J. R.; Knafla, R. T.; Maye, P. V.; Nikolaides, N.; Oneyemi, F. Y.; Parkhurst, G. J.; Pecore, S. E.; Reiter, M. J.; Testerman, L. S.; Thompson, N. J.; Wagner, T. L.; Weeks, C. E.; Andre, J.-D.; Lagain, D.; Bastard, Y.; Lupu, M. Synthesis and structure−activity-relationships of 1*H*-Imidazo[4,5-*c*] quinolines that induce interferon production. *J. Med. Chem.* **2005**, *48*, 3481−3491.
(37) Laxer, A.; Major, D. T.; Gottlieb, H. E.; Fischer, B. (^{15}N5)-Labeled adenine derivatives: synthesis and studies of tautomerism by ^{15}N NMR spectroscopy and theoretical calculations. *J. Org. Chem.* **2001**, *66*, 5463−5481.
(38) Carson, D. A.; Takabayashi, K.; Cottam, H. B.; Chan, M.; Wu, C. C. N. TLR Agonists. U.S. Patent 71,033,705 P, Aug 22, 2005.
(39) He, L.; Gangwar, S.; Poudel, Y. B.; Sivaprakasam, P. Toll-like Receptor 7 (TLR7) Agonists Having Heteroatom-Linked Aromatic Moieties, Conjugates Thereof, and Methods and Uses Therefor. U.S. Patent 20,190,055,247 A1, Feb 21, 2019.
(40) Hirota, K.; Kazaoka, K.; Sajiki, H. Synthesis and biological evaluation of 2,8-disubstituted 9-benzyladenines: discovery of 8-mercaptoadenines as potent interferon-inducers. *Bioorg. Med. Chem.* **2003**, *11*, 2715−2722.
(41) Karroum, N. B.; Moarbess, G.; Guichou, J.-F.; Bonnet, P.-A.; Patinote, C.; Bouharoun-Tayoun, H.; Chamat, S.; Cuq, P.; Diab-Assaf, M.; Kassab, I.; Deleuze-Masquefa, C. Novel and selective TLR7 antagonists among the imidazo[1,2-*a*]pyrazines, imidazo[1,5-*a*]-quinoxalines, and pyrazolo[1,5-*a*]quinoxalines series. *J. Med. Chem.* **2019**, *62*, 7015−7031.
(42) Shukla, N. M.; Mutz, C. A.; Malladi, S. S.; Warshakoon, H. J.; Balakrishna, R.; David, S. A. toll-like receptor (TLR)-7 and -8 modulatory activities of dimeric imidazoquinolines. *J. Med. Chem.* **2012**, *55*, 1106−1116.
(43) Veber, D. F.; Johnson, S. R.; Cheng, H.-Y.; Smith, B. R.; Ward, K. W.; Kopple, K. D. Molecular properties that influence the oral bioavailability of drug candidates. *J. Med. Chem.* **2002**, *45*, 2615−2623.
(44) Smith, D. A.; Beaumont, K.; Maurer, T. S.; Di, L. Volume of distribution in drug design. *J. Med. Chem.* **2015**, *58*, 5691−5698.
(45) Hawkes, J. E.; Adalsteinsson, J. A.; Gudjonsson, J. E.; Ward, N. L. Research techniques made simple: murine models of human psoriasis. *J. Invest. Dermatol.* **2018**, *138*, e1−e8.

https://dx.doi.org/10.1021/acs.jmedchem.0c00011
J. Med. Chem. 2020, 63, 4776−4789